Bio-functionalization, stabilization and potential functionalities of hyaluronate macromolecules capped copper oxide nanoparticles

Tijo Cherian[1*], Chinnasamy Ragavendran[2], Roshan K V Remesh[3], Wajih Jamal[4], Jenny Jacob[1], Chinnaperumal Kamaraj[5] , Ismini Nakouti[6***]**

[1]School of Biosciences, Mar Athanasios College for Advanced Studies Tiruvalla (MACFAST), Tiruvalla, Kerala-689101, India

[2]Department of Conservative Dentistry and Endodontics, Saveetha Dental College and Hospitals, Saveetha Institute of Medical and Technical Sciences (SIMATS), Chennai, India

[3]Department of Biotechnology, Sree Narayana Arts and Science College, Kumarakom, Kottayam, Kerala- 686563, India

[4]Department of Zoology, Aligarh Muslim University, Aligarh, Uttar Pradesh, India 202002

[5]Interdisciplinary Institute of Indian System of Medicine (IIISM), SRM Institute Science and Technology, Kattankulathur-603 203, Tamil Nadu, India

[6]Centre for Natural Products Discovery (CNPD), School of Pharmacy and Biomolecular Sciences, Liverpool John Moores University, Liverpool L3 3AF, UKE. mail: I.Nakouti@ljmu.ac.uk

***Corresponding authors:**

1. **Tijo Cherian**: School of Biosciences, Mar Athanasios College for Advanced Studies Tiruvalla (MACFAST), Tiruvalla, Kerala-689101, India. E.mail: tvarghese891@gmail.com.

2. **Chinnasamy Ragavendran**: Department of Conservative Dentistry and Endodontics, Saveetha Dental College and Hospitals, Saveetha Institute of Medical and Technical Sciences (SIMATS), Chennai, India. E. mail: ragavan889@gmail.com.

3. **Ismini Nakouti:** Centre for Natural Products Discovery (CNPD), School of Pharmacy and Biomolecular Sciences, Liverpool John Moores University, Liverpool L3 3AF, UK E.mail: I.Nakouti@ljmu.ac.uk

Abstract

The optical-electrical properties of CuO-NPs (copper oxide nanoparticles) are being expanded widely for high-technological uses. In accordance with the idea of an eco-friendly synthesis process, CuO-NPs were synthesized utilizing a safer method; stabilized by biopolymer sodium hyaluronate (SH) rather than a hazardous substance. Using one variable at one time method with constant reaction variables, the synthesis parameters were optimized and the characteristics of CuO-NPs were controlled. The resulting particles exhibited restricted distribution, were typically round or oval in form and particle size of 17±1.3 nm (by TEM and SEM), strongly crystalline (by XRD) and were noticeably stable. The experimental analysis of FT-IR documented that the redox reaction between biopolymers and metal cations; coupled by capping effect of thin layer of SH-macromolecules, are primarily responsible for the formation and stabilization of CuO-NPs. Also, CuO-NPs exhibited strong bactericidal (ZOI 22-27 nm; antibiofilm potential 71-85%), anti-diabetic (70-72%), DNA cleavage and antioxidant activity (70-85%). Additionally, SH-stabilized CuO-NPs demonstrated catalytic activity for the reduction of catalytic dyes, degrading at a rate of over 91-93% in about 10 to 20 min. The current synthetic technique may be applied consecutively to synthesize catalytically active CuO-NPs which exhibited remarkable *in-vitro* biological and biomedical capabilities, possessing the potential to be exploited as a broad-based agent in a variety of biomedical and industrial processes, including the treatment of wastewater.

Keywords: Sodium hyaluronate, CuO-NPs, Wastewater treatment, Dye degradation, Antioxidant, Antibacterial activity

1. Introduction

With numerous applications spanning from engineering to health, nanotechnology has emerged as one of the most inventive domains of science and technology [1]. These nanoscale materials have been fabricated using a variety of techniques, including physical, chemical, and environmentally friendly ways; however, these techniques have many shortcomings. Due to their biocompatibility, safety, low toxicity, and cost-effectiveness, green approaches have replaced previous conventional manufacturing techniques for nanoparticles (NPs) over the past few decades [2,3]. The term "Green" refers to the usage of plant-based materials, and “Green nanotechnology” is a subfield of green technology that draws on the ideas of green engineering and green chemistry [4]. Through the use of fewer resources and renewable variables, it decreases the consumption of fuel and energy. Furthermore, by conserving water, energy, and raw materials, as well as by lowering emissions of greenhouse gases and toxic waste; nano-technological goods, procedures, and uses are anticipated to greatly contribute to climatic and environmental protection [1]. The key benefits of green nanotechnology include increased energy efficiency, reduction in waste and emissions of greenhouse gases, and reduced utilization of non-renewable resources. Now-a-days, eco-benevolent nanotechnology syntheses entail the production of NPs without the use of toxic materials that result in harmful byproducts. In other words, the sustainable technique is a way to synthesize nanoparticles that are eco-friendly and doesn't harm biodiversity or human health. It is entirely plausible that current conventional manufacturing processes can produce NPs with exact morphology and size in vast quantities. These techniques, however, use time-consuming, difficult, toxic, and expensive manufacturing methods [5]. Green approaches have many advantages over

78 traditional physical and chemical methods, including quick, simple manufacturing
79 protocols, ease of use, economy, and less waste product formation [6]. Green
80 engineering and chemistry are the foundations upon which green nanotechnology is
81 built, rather than ascend de novo. Green nanotechnology applications could include the
82 utilization of nanomaterials in clean production procedures that synthesize
83 nanoparticles using solar radiations or recycling industrial waste products into
84 nanomaterials, besides the development of fuel cells, biofuels, and solar cells [1,4].
85 There is some "truly" green nanotechnology, such as the full growth of nanoparticles in
86 plants, but these efforts are unlikely to achieve the scale needed for the manufacture of
87 nanomaterials on industrial scale. Green nanotechnology requires a thorough process
88 evaluation in order to get definitive outcomes, much like other industrially produced
89 goods.

90 One of the most practical possibilities among the green approaches available is
91 the biological reduction of metallic cations to neutral ions; subsequent stabilization
92 utilizing a natural template. In order to keep the particle exceedingly stable and
93 catalytically effective by preventing aggregation, this technique normally requires the
94 addition of a template or supporting agent [7]. The employed biotemplate can be
95 derived from biological polymers, dendrimers, organic ligands, plants, different
96 polysaccharides [8,9]. Plant phytochemicals require a supplementary process in the
97 extraction of required substances pre-application because they contain more active
98 components than chemical approaches do. It is difficult to separate and purify
99 manufactured nanoparticles from plant matter [10,11]. In addition, other
100 environmentally friendly synthesis methods, such the production of nanomaterials with
101 the assistance of microorganisms, are ineffective and expensive because to the need for
102 special tools to handle the microbes. According to this theory, naturally occurring

carbohydrates that are readily available, for example glucose, pectin, starch, chitin, agar, maltose, arabinose provide a much better starting point in the synthetic process of metal nanoparticles [12]. Such carbohydrate polymeric substances which have large number of structurally bound hydroxyl and carboxylic groups can reduce the metallic salts while also stabilizing the produced nanoparticles. Many scientific literatures have reported a variety of types of carbohydrates, including alginate, chitosan [13-15], carrageen [16,17], cellulose [18], and konjac [19,20], in the fabrication of very stable metal nanoparticles with no aggregation, homogeneous shape and size, high crystallinity, and good catalytic reduction efficiency [21]. The goal of the present work is to develop catalytically efficient CuO-NPs based on sustainable chemistry principles by investigating how SH functions as a stabilizer and reductant of metal precursors.

Sodium hyaluronate (SH), classified as glycosaminoglycan, is a long-chain dense biopolymer made of disaccharide monomers of Na-glucuronate-N-acetylglucosamine [22]. It has a variety of uses, including medications (intra-articular injection, creams, etc.), food manufacturing (dietary management for maintaining the amount of carbohydrates), plastic surgery of the skin, and cosmetics for wound healing [21]. In addition to these applications, given that they include a significant amount of hydroxyl and carboxyl groups, it can also be utilized to stabilize metallic particles during the production of nanoparticles. Moreover, SH has been extensively researched for its functions as a template, stabilizer, and reductant for the synthesis of metallic nanoparticles. For instance, SH conjugated metallic nanoparticles have been reported in wide ranging applications like (i) SH-reduced iron oxide nanoparticles for tracking medication and imaging delivery to cancerous cells [23]; (ii) SH-ZnONPs as anti-tumors [24] and wound healing relevance [25]; (iii) SH-AgNPs matrices for antibacterial activity [26]; (iv) chemical reduced SH templated AgNPs in biosensing [27]; (v) AgNPs

decorated SH fibers in wound dressing and healing [28]; (vi) cetyl trimethyl ammonium bromide (CTAB)-SH stabilizer in the fabrication of silver nanowires [29];(vii) SH capped silver nanoparticles for in-vivo imaging [30]; (viii) Tween 80 coupled SH in the synthesis of nano silver for cellular level targeted drug delivery [31]. To the best of the authors' knowledge, there has never been an easy-to-read study explaining wide applicative insights with CuO-NPs that have been reduced and stabilized using a sustainable synthesis procedure. The few relevant works on SH-assisted metal nanoparticles that have been published should be noted; nonetheless, their synthesis processes and end products differ greatly from those of our study. For exemplar, (i) SH-capped nanogold was synthesized by employing the technique of γ -irradiation [32]; (ii) SH assembled gold nanoclusters were fabricated by photodynamic ablation [33]; (iii) glycosaminoglycans stabilized AgNPs were applied as an efficient anti-coagulant and anti-inflammatory agents [34]. Therefore, it is evident that SH-assisted CuO-NPs have not been reported for wide scale applications in various biological fields.

Due to their large surface area and small size, metallic nanoparticles have a wide range of uses. Among metal or metal-based nanoparticles, CuO-NPs (copper oxide nanoparticles), a type of metallic nanoparticle, have been applied in a variety of fields, such as catalysis, textile, biomedical, and biosensing [35-38]. Additionally, CuO is more affordable than silver, mixes well with polymers, and has relatively stable physical and chemical characteristics. For the generation of CuO-NPs, a variety of natural sources, such as plants, microorganisms, and fungus, are used [39,40]. Vitamins, carbohydrates, phenolics, and flavonoids are few of the biomolecules and metabolites found in plant extract. These substances have the ability to reduce and stabilize substances as well as convert Cu^{2+} ions into CuO-NPs [41]. Free radical overproduction in the body is a major

153 factor in the development of degenerative conditions like cancer, cataracts,
154 cardiovascular disease, brain dysfunction, and a weaker immune system [42].
155 Antioxidants can, however, neutralize these free radicals before they assault bodily cells
156 and cause disease. Particularly well-known for efficiently scavenging oxygen-
157 containing free radicals are CuO-NPs [43]. Due to their large surface areas and peculiar
158 crystal surface morphologies, metal and metal-based nanoparticles are of great
159 significance. Along with their antioxidant properties, CuO-NPs also have antibacterial
160 properties that are effective against pathogenic bacterial strains [1, 3, 44].

161 Textile manufacturing units are one of the largest sources of wastewater and
162 effluents since they use enormous volumes of synthetic dye compounds, solvent, and
163 auxiliaries during various processing steps [45, 46]. Approximately, 5000 tons of dyes
164 and its auxiliaries are discarded into the aquatic environment each year due to the huge
165 volumes of effluents' unsuitability for reuse. These effluents are extremely poisonous,
166 aesthetically detrimental, mutagenic and carcinogenic in nature [47]. Strong colour,
167 high TDS (total dissolved solids), high chemical oxygen demand (COD), limited
168 biodegradability and changing pH are some of the characteristics of this effluent [21].
169 The textile units frequently modify the dyeing process's colour palette, which results in
170 considerable modifications to the properties of effluents, particularly in terms of COD,
171 pH, colour, and turbidity [48]. Additionally, even if the dye-contaminated effluents
172 undergo small level breakdown, dye molecules are structurally stable creating harmful
173 poisonous chemicals including benzidine, naphthalene, and other aromatic compounds
174 [21]. Many governments enact strong regulations to prevent the use of harmful colours
175 (such azo) and uphold minimum standards for water quality before discharges. Alas,
176 the realistic usage of such dangerous dye compounds has not been eliminated because
177 of their accessibility, cost-compatibility, and remarkable dyeability [1]. As remedial

steps, the most popular technique for treating industrial wastewater flocculation or coagulation have been in practice since it efficiently tackles the problems of turbidity, odour, and colour and is straightforward in application [49]. However, there are significant disadvantages to this conventional approach for treating textile wastewater, including high energy and chemical consumption as well as outlay expenditure for the dosage per tank units. Additionally, it creates sludge, which needs additional treatment before disposal because it is regarded as a secondary contaminant [50]. As a result, the treatment of raw textile industry effluents has become urgently in need of an integrated process. As an alternative, advanced technology known as catalytic oxidation has lately been used to decompose poisonous and dangerous organic contaminants [51, 52]. Additionally, it is used in the decomposition of lignin in wood pulp and unwanted stains on clothing. Recent years have seen a substantial increase in research into metallic and metallic oxide derived nano catalysts utilized in the catalytic degradation of pollutants in both scientific and industrial worlds [53]. This is a result of their special characteristics such as high catalytic effectiveness, high surface area to volume ratio, efficient active site diffusion, simple scattering of the reactants to the surface of nanoparticles and simple elimination of contaminants from the solution [1]. Additionally, recent advances in nano catalysts and nanomaterials were thoroughly investigated, and their potential applications in water purification, wastewater remediation, biosafety, toxicity, and other fields [54, 55]. When compared to other nanomaterials, copper oxide nanoparticles (CuO-NPs) as nano catalysts stand out due to their unique and promising characteristics, such as a simple manufacturing technique, effective catalytic activity, nanoscale dimension, and improved optical behavior [56-58]. Herein, the current study aims to use sodium hyaluronate as a capping/reducing agent in the biosynthesis of CuO-NP and to scrutinize the potential of

SH assisted CuO-NPs for myriad biological applications. This is the first investigation on the synthesis of copper oxide nanoparticles using SH. The CuO-NPs were examined for their biological potential utilizing a variety of in-vitro assays, spectroscopic and analytical methods. Additionally, the biosynthesized CuO-NPs were used to investigate the antioxidant and dye degradative efficiency in order to forecast their potential for pharmaceutical use and water treatment practices.

2. Materials and methods

2.1 Chemicals

Sodium hyaluronate (SH; molecular weight, Mw = 300000 g/mol), copper acetate monohydrate (Mw = 199.65 g/mol), sodium borohydride ($NaBH_4$), nutrient broth (NB), Mueller–Hinton agar (MHA) and sodium hydroxide (NaOH) was purchased from Sigma Aldrich. The molecular grade absolute ethanol, model azo dyes [RY145 (reactive yellow 145) and RR195 (reactive red 195)], were purchased from Hi-Media, India. All chemicals used in the study were 97-98% in purity and the respective solutions were prepared using sterile distilled water.

2.2. Synthesis of SH-assisted CuO-NPs

The aqueous solution of SH was prepared by cautiously mixing powdered SH into sterile distilled water under continuous swirling by vortex mixer. (Since, SH is sparingly water soluble, it binds to water molecules instantaneously forming gel). Therefore, the initial mixture was constantly stirred till no visible lumping. Following, the prepared SH solution was mixed with metal solution of copper acetate. Various temperature of temperature-controlled water was applied to the combined solution for a predetermined amount of time. The process parameters were methodically investigated one aspect at a time in order to regulate the final characteristics of

synthesized CuO-NPs and optimize the synthesis conditions. The variables were: reaction temperature (30, 40, 50, 60, 70˚C), reducing/stabilizing agent concentration (0.05, 0.10, 0.15, 0.20, 0.25%), incubation duration (10, 20, 30, 40, 50 min), and solution pH (4, 6, 8, 10, 12). The final step was to cool and store the synthesized CuO-NPs at room temperature for 24 hours till further characterization. This was done in accordance with the determined optimal conditions, which called for heating a combination of 0.1 mM copper acetate and 0.15% SH for 40 min at 50˚C.

2.3. Characterization and measurement

The characterization techniques of ultra-violet visible spectrophotometer, XRD (X-ray diffraction), FT-IR (Fourier transforms infrared spectroscopy), SEM (scanning electron microscopy), high-resolution TEM (transmission electron microscopy), EDX (energy disperse X-ray spectroscopy) were used to characterize CuO-NPs synthesized under ideal conditions. To calculate the efficiency of the catalytic process, the degradation of the azo dye in the presence of CuO-NPs and sodium borohydride was studied. The characterization methods and instrument requirements followed the guidelines mentioned in our earlier report of [1].

2.4 Anti-diabetic potential of CuO-NPs

2.4.1 α-Amylase inhibition assay

α-amylase inhibition test was determined for analyzing the anti-diabetic potential of CuO-NPs [59]. In brief, 25 µl of α-amylase enzyme (0.14 U ml^{-1}) +15 µl phosphate buffer (pH 6.8) were mixed in a sterile 96 well plate. Following, CuO-NPs (10 µl; concentrations 20-100 µg/ml) and starch solution (40 µl) were mixed and incubated for 30 minutes at 50˚C.Post incubation, iodine reagent (90 µl; 5 mM potassium iodide, 5 mM iodine) and 1M HCl (20 µl)were added to the resulting mixture. The reaction

controls: positive control (acarbose); negative control (solution without test sample) and blank (solution devoid of CuO-NPs and enzyme) were taken in parallel. The optical density of reaction solution was measured at 595 nm and the % enzyme inhibition was evaluated by using following equation (Eq. 1):

$$\%\ Enzyme\ inhibition = OD(s) - \frac{OD(n)}{OD(b)} \times 100 \quad \text{------- (Eq. 1)}$$

where OD (n) stands for a negative reference, OD (b) for a blank, and OD (s) for the test sample's absorption value.

2.4.2 *In vitro* α-glucosidase inhibition assay

The α-glucosidase inhibition potential of CuO-NPs was ascertained by the protocol of [60] with slight alterations. The reaction mixture: α-glucosidase (7.5 µl; stock solution (0.5 U/ml) in 20 mmol/l sodium phosphate buffer, pH 6.9) mixed with SH, CuO-NPs (20-100µg/ml) and acarbose was kept at 37°C for 15 min. Further, p-nitrophenyl-α-glucopyranoside (PNPG; 100µl) was added followed by incubation for 10 min at 37°C. Finally, sodium carbonate (Na_2CO_3) (100µl; 0.1 M) was mixed to arrest reaction. The absorbance values were read at 405 nm and acarbose was used as reference and control (PNPG + α-glucosidase).

$$\%\ inhibition = \frac{control\ OD - test\ OD}{control\ OD} \times 100 \quad \text{------- (Eq. 2)}$$

2.4.3 Non-enzymatic a-glycosylation of hemoglobin (HbA1c)

The biosynthesized CuO-NPs were used in a typical HbA1c inhibition test utilizing the HbA1c technique, with slight modifications [61]. Using 0.01 M phosphate buffer (pH 7.4) as the reaction medium, the arrangement of glucose (2%), haemoglobin (0.06%), and sodium azide (0.02%) were thoroughly mixed. At room temperature, different concentrations of CuO-NPs (20-100 µg/ml) were mixed with the preceding

response mixture. The completed reaction mixture was incubated at room temperature for 72 h under dark environment. The levels of HbA1c inhibition were read at 520 nm and contrasted with those of a common medication like metformin.

2.4.4 Urease inhibition assay

To ascertain urease inhibition activity [62], the reaction mixture (10 µl CuO-NPs, phosphate buffer (50 µl,3 mM, pH 4.5), 100 mM urea, 25 µl urease) was incubated for 15 minutes at 30°C. Post incubation, 1µl sodium nitroprusside 0.005% (w/v) and 45 µl phenol reagent (phenol 1% (w/v) was added, following the addition of alkali reagent (70 µl; 0.5% NaOH and 0.1% NaOCl) and incubation at 30°C for 50 minutes. The reaction controls: positive control (thiourea); and blank (solution without CuO-NPs) were taken in parallel. The optical density was measured at 630 nm and % inhibition of urease was evaluated by following equation (Eq. 3):

$$\%\ Enzyme\ inhibition = OD(b) - \frac{OD(s)}{OD(b)} \times 100 \quad \text{-------- (Eq. 3)}$$

where OD (b) stands for "blank" and OD (s) for "test sample value."

2.4.5 Lipase inhibition assay

The lipase inhibition assay was ascertained following the slight modified procedure of [63]. The enzyme lipase (10 mg ml^{-1}) in aqueous state was subjected to vortex (6,000 rpm; 5 min.) and the resultant supernatant was rescued. The reaction mixture [Tris buffer (350 µl;100 mM; pH 8.2), 150 µl lipase and CuO-NPs (50 µl)] was taken and mixed with substrate (olive oil; 450 µl) in order to initiate the reaction and incubated at 37°Cfor 120 min. Post incubation, the solution was centrifuged (16,000 rpm; 5 min.) and the optical density was read at400 nm by taking 200 µl of the resulting supernatant. The reaction controls: blank [buffer (400 µl), lipase (150 µl), and substrate

298 (450 µl)] and positive control (orlistat) were running parallel. The percent inhibition of
299 enzyme was evaluated by equation (Eq. 3).

300 **2.5 Antioxidant activities of biosynthesized CuO-NPs**

301 **2.5.1 Free radical scavenging assay (FRSA)**

302 The DPPH (2,2-diphenyl 1-picrylhydrazyl) assay was performed for the
303 assessment of free radical scavenging potential of CuO-NPs [64]. Briefly, 10 µl CuO-
304 NPs+ 190 µL DPPH reagent were mixed and kept for 30 min at 37°C. Ascorbic acid was
305 act as positive control. The absorbance of reaction solution was recorded at 515 nm and
306 the following equation (Eq. 4) was used to estimate the scavenging activity:

307 $$\%\ Scavenging = \left(1 - \frac{AE}{AD}\right) \times 100$$ ------- (Eq. 4)

308 where AE directs absorbance of test sample solution and AD denotes negative control.

309 **2.5.2 Total antioxidant capacity (TAC)**

310 The total antioxidant capacity of CuO-NPs was quantified by using
311 phosphomolybdenum method [65]. Briefly, 900 µl phosphomolybdenum reagent
312 [sulphuric acid (0.6 M), ammonium molybdate (4 mM), and sodium phosphate (28
313 mM)]+ 100 µl CuO-NPs was mixed and kept for 90 min at 95°C. Post incubation, the
314 absorbance of the reaction mixture (volume 200 µl) was read at 695 nm. The antioxidant
315 potency was ascertained as the amount of ascorbic acid equals to ascorbic acid per mg
316 of test sample (mg AAE/mg).The positive reference employed was ascorbic acid.

317 **2.5.3 Total reducing power (TRP)**

318 The total reducing power of CuO-NPs was investigated by potassium
319 ferricyanide based assay [65]. Iron, as reducing agent, was used for the quantification of

total reducing power. The reaction mixture: 40 µl CuO-NPs + phosphate buffer (400 µl, 0.2 mol/l, pH 6.6) + aqueous potassium ferricyanide (1%) was kept at 45°C for 20 min. Post incubation, aqueous trichloroacetic acid (400 µl; 10%) was added and mixed in the resulting mixture; centrifuged at 3000 rpm for 10 min. The resultant supernatant (volume 500 µl) was added with equal volumes of 100 µl aqueous $FeCl_3$ (0.1%) and sterile distilled water. The absorbance (630 nm) was read and the outcomes were quantified as mg AAE/mg. The reaction controls: positive control (ascorbic acid) and blank (DMSO) were run in parallel.

2.5.4 ABTS antioxidant assay

The ABTS assay was investigated by following the protocols of [66]. The reaction mixture [equal proportions of 7mM ABTS salt and potassium persulphate (2.5 mM)] was kept under dark conditions for 14-16 h. Prior to the addition of CuO-NPs, the absorbance (734 nm) was read and adjusted to 0.7. The variable concentrations of CuO-NPs were then added to the reaction mixture and kept for 15 min at room temperature under dark conditions. The antioxidant effect has been detected in TEAC and the absorption was measured at 734 nm (trolox C equivalent antioxidant capacity, mM).

2.5.5 FRAP (ferric reducing antioxidant power) assay

The ferric reducing power was investigated as developed by [67]. 10 µl CuO-NPs was added to 190 µl FRAP solution [TPTZ (2,4,6-tri(2-pyridyl)-s-triazine; 10 mM); acetate buffer (300 mM; pH 3.6); $FeCl_3.6H_2O$ (ferric chloride hexahydrate; 20 mM) in the ratio 10 : 1 : 1 (v/v/v)] and kept for 15 min. at room temperature. The O.D (630 nm) was recorded and the reducing antioxidant effect was determined as TEAC.

2.5.6 Nitric oxide scavenging activity

Nitric oxide (NO_2) scavenging capacity was measured by the procedure of [68]. Briefly, different CuO-NPs concentrations (20–100µg/ml) were mixed with sodium nitroprusside solution (10 mM) and kept for 2.5 h at 25°C. Following incubation, the reaction solution (0.25 ml) was mixed with sulfanilic acid and n-1-naphthyl indicator (0.5%; 0.5 ml) and kept at 25°C for 30 min. The absorbance was read at 540 nm and the % scavenging activity was evaluated by the following equation (Eq. 5):

$$Scavenging\ activity\ \% = \frac{Abs\ (control) - Abs\ (sample)}{Abs\ (control)} \times 100$$ -------- (Eq. 5)

where Abs control and Abs sample stand for the relative absorption of the control and sample.

2.5.7 Hydrogen peroxide radical scavenging (H_2O_2) assay

The H_2O_2 scavenging capacity of CuO-NPs was ascertained by the protocol of [69]. The reaction solution consisted of hydrogen peroxide (40 mM) in phosphate buffer (50 mM, pH 7.4) was prepared. The H_2O_2 concentration was determined at wavelength 230 nm. The resulting combination was mixed with aqueous CuO-NPs (20–100 µg/ml) and allowed to stand at room temperature for 30 min. The reaction solution was measured at 230 nm in comparison to a blank solution (phosphate buffer without hydrogen peroxide), and the equation was used to determine the percentage of hydrogen peroxide scavenging (Eq. 5).

2.6 Measurement of peroxidase-like activity of CuO-NPs

The POD (peroxidase) activity was ascertained as described by [70]. Briefly, the reaction mixture: 140 µl NaAc–HAc buffer (0.2 M, pH 4.0) + 20 µl CuO-NPs were mixed thoroughly with the subsequent addition of freshly prepared H_2O_2(6 mM) and freshly prepared TMB (3 mM, 20 µl). The absorbance (652 nm) was read and the reaction

366 combination (with no test sample) was taken as control. The enzymatic activity was
367 determined by using equation (Eq. 6):

368 $$A = ELC$$ ------- (Eq. 6)

369 where A denotes the sample absorption value, C the enzyme content (measured in
370 millimolars per milligram), E the extinction coefficient, and L the wall length,
371 correspondingly.

372 **2.7 Detection of reactive oxygen/nitrogen species**

373 The generation of reactive species (ROS and RNS) by CuO-NPs was reported by
374 using fluorescent dye DHR-123 (dihydrorhodamine-123) [67]. Yeast cells, in existence of
375 CuO-NPs and control (DMSO), was incubated for overnight under dark at 30°C for 10
376 min. Post incubation, the cells were cleaned with PBS thrice and re-suspended in 0.4 μM
377 DHR-123 dissolved in PBS. The fluorescence wavelengths λ_{ex} = 505 nm, λ_{em} = 535 nm
378 were used to detect the fluorescence by BioRad Versa Fluor Fluorimeter.

379 **2.8. Metal chelating activity**

380 The metal ion chelating property of SH assisted CuO-NPs were quantified. The
381 reaction mixture consisting of: $FeSO_4$ (1ml) + CuO-NPs (20-100μg/ ml) + solution of 2,2′-
382 bipyridyl (1ml) and Tris- HCl buffer (pH 7.4) + mixture of ethanol and hydroxyl amine-
383 HCl. The reaction mixture (5ml) was maintained for 10 min at room temperature. The
384 O.D values was read at 522 nm and the ion chelating activity was measured by Eq.(5)
385 [71].

386

387 **2.9Assessment of Antibacterial activity of CuO-NPs**

388 **2.9.1. Maintenance of pathogenic strains**

Two bacterial pathogens, namely, *Escherichia coli* and *Staphylococcus aureus* were sub-cultured periodically on MHA and maintained as culture stock in form of 10% glycerol stocks (-20°C) and slants at (4°C).

2.9.2. Minimal Inhibitory Concentration (MIC) and Minimal Bactericidal Concentration (MBC) of CuO-NPs

For evaluation of MIC, broth micro-dilution technique was employed [1, 72]. The variable concentrations of CuO-NPs (20-100μg/ml) were tested; maintained for 24 hat 37°Calong with control tubes. The optical density was measured at 620 nm. For assessment of MBC, aliquots (20 μl) from MIC tubes assay were seeded, cultured on NA medium followed by incubated for 24h at 37°C [3, 73].

2.9.3. Antibacterial activity of CuO-NPs

The bactericidal effects of CuO-NPs was performed by using agar well diffusion technique [1, 74, 75] against human pathogens (*E. coli* and *S. aureus*).The bacterial culture (0.1 ml; cell density 2×10^8 CFU/ml) were lawn spread uniformly on MHA media. Equal sized wells were made and variable concentrations of CuO-NPs (20, 60, 80, and 100μg/ml) were added to the former and stored at 37°C for 24 h. The antibiotic cefixime act as positive control and the size of zone of inhibition (ZOI) was calculated by antimicrobial zone measurement scale (Hi-Media, India).

2.9.4. Anti-biofilm potential of CuO-NPs

The anti-biofilm efficacy of CuO-NPs was analyzed by employing CV (crystal violet) assay [1]. Starter cultures (100 μl; cell density ~10^8 cells/ml) of *S. aureus* and *E. coli*, grown overnight in NB, were seeded into 96-well microtitre plate. A 100 μl culture medium + variable CuO-NPs concentrations (100 μl; 20–100μg/ml) was dropped to the respective wells along with a parallel set of untreated culture run as control followed by

cultivation for 24 h at 37°C. The remaining loosely bound cells were washed thrice with PBS (phosphate buffer saline) + autoclaved distilled water (1:1). The CV solution (0.25%, 200µl) was added followed by incubation for 30 min at 37°C. The unbound CV was washed with PBS + autoclaved distilled water. The bound CV-bacterial cells were dissolved in ethyl alcohol (95%; 250 µl) and the absorbance read at 620 nm using ELISA reader.

2.10. DNA cleavage assay

The CuO-NPs treated vector pBR322 DNA was examined as described by [76]. Aliquots (50 µl) of SH and CuO-NPs (20, 60, 100 µg/ml) solutions were separately added to vector DNA (1µl; 0.5 µg/ml)in TE buffer (0.1 mM EDTA, 10 mM Tris–HCl, pH 7.4) followed by incubation at 37°C for 24 h under dark. Consequently, gel electrophoresis (1% agarose gel) was ran by using 20 µl copper acetate and CuO-NPs–bacterial DNA mixtures each and viewed using UV light trans-illuminator equipped gel documentation system.

2.11. Mechanism of action of CuO-NPs on treated bacterial cells

2.11.1. Protein leakage assay

The estimation of cellular protein leakage was ascertained by previously developed protocol of [77]. The CuO-NPs (MIC concentration) treated bacterial cells were incubated for fixed time intervals of 3h and 6h and then centrifuged at 6000 rpm for15 min. For each ensuing sample, the Bradford reagent (800 µl) + supernatant (200 µl) were mixed; followed by incubation for 10 min at room temperature. The protein BSA served as standard for the measurement of optical density (λ 595 nm).

2.11.2. Nucleic acid (NA) leakage assay

The quantification of NA leakage was ascertained by the protocol of [78]. Aliquots of CuO-NPs (MIC concentration) treated bacterial cultures were incubated for fixed time intervals of 3h and 6h followed by filtration by Millex-GS syringe filters (Millex-GS, Spain) using dimension: diameter 25 mm; pore size 0.2 μm. The values of absorbance were measured at 260 nm.

2.12. Brine shrimp lethality assay for cytotoxicity test

The precursive cytotoxicity of CuO-NPs was determined by employing brine shrimp lethality assay [79]. The medium comprising of artificial seawater (34 g sea salt + 1.0 liter sterile distilled water under incessant stirring) was used for hatching eggs of *Artemia salina* (brine shrimp) between 28±2.0°C. After egg hatching, 5 ml brine was added to the test CuO-NPs concentrations. Post 2 days, hatched shrimps were transferred to the test CuO-NPs concentrations (15 shrimps/concentration). After 24 h, the number of surviving shrimps was recorded and the percentage viability was calculated based on the following method (Eq. 7):

$$Percentage\ viability = \frac{control - test}{control} \times 100 \text{ -------- (Eq. 7)}$$

2.13. Dye degradation and kinetics study

The degradation of azo-dyes (RR195 and RY145) was calculated using optimized SH-assisted CuO-NPs as nanocatalysts using $NaBH_4$ [21]. For experiment, dye (10 mg each) + 1.0 liter sterile distilled water were mixed; accounting stock solutions for two separate simulated wastewater samples. The CuO-NPs (20 ml) were added and mixed with 10 ml as-prepared simulated wastewater and 100 ml aqueous $NaBH_4$ solution (0.1mol/l). The resulting solution was well mixed by manual shaking, and the UV-Vis absorption spectra were promptly read at room temperature. The catalytic degradation

was measured by recording time-dependent change in the absorbance. A common equation (Eq. 8) was used to measure the amount of dye degradation (D%):

$$D\% = \frac{(Ao - At)}{Ao} \times 100 \text{ ------- (Eq. 8)}$$

where At denotes absorption at a specific time and A0 denotes starting absorbance. (t). The rate constant was evaluated by typical kinetic equation (Eq. 9):

$$\ln\left(\frac{At}{Ao}\right) = -kt \text{ ------- (Eq. 9)}$$

where k corresponds to the kinetic degree constant, t indicates reduction time, A_0 was the measure of initial spectrum , and A_t was the measure of absorbance of dyes at time t.

2.14. Statistical analysis

All investigations were performed in triplicates and the data were interpreted as mean ± S.D. calculated by using SPSS (Version 7.5.1, USA). The results of inhibition assays; peroxidase and ROS/RNS activity were evaluated by One-way ANOVA (analysis of variance) followed by unpaired Bonferroni test. The *p* value <0.05 indicated the arithmetical significance of results.

3. Results and Discussion

The current study employs sodium hyaluronate as stabilizing and reducing agent in the synthesis of copper oxide nanoparticles. In study, the sodium hyaluronate was chosen as the base material owing to its attributes of naturally occurring polymer that gels in the presence of a cross-linker sans the need for organic solvents or extremely high temperatures. This function conveniently prevents the loss or destruction of labile medications [80, 81]. Also, the molecules of hyaluronate are biocompatible and encourage interaction of biological cues with particular cellular receptors [82].

3.1. Synthesis and optimization of SH- assisted CuO-NPs

The formation of SH-CuONPs was preliminary inveterate by the visual color shifted of the reaction mixture. An aqueous solution of SH is colorless, while the solution of copper acetate [$Cu(OAc)_2$] was found to be blue colored. However, the color of the reaction mixture changed under thermal heating, depending upon the reaction parameters. The coupled oscillation of free electron conduction, induced by LSPR representing the production of CuO-NPs, is responsible for the development of vivid colour [3, 83]. The size and form of the colloid's particle were linked to the variations in colour as the literature states that colour change from bluish green to grayish black are suggestive of the formation of colloidal CuO-NPs at the nanoscale [3]. The spectroscopic analysis of the colloid reaction mixture validated the development of CuO-NPs (Fig. 1a). The absorption peak at 244 nm of copper acetate was recorded primarily due to LMCT transition (ligand-to-metal-charge-transfer) of AcO^- ions and d-d transition of Cu^{2+} ions. On the other hand, no absorptive peak was exhibited by SH under observed wavelength range. However, heating at ambient conditions caused the dissipation of UV-Visible absorption peak of $Cu(OAc)_2$ at 244 nm indicating the reduction of Cu^{2+} into Cu^0 [83]. The generation of CuO-NPs was exhibited by the concurrent peak appearance at 575 nm and a strong plasmonic peak band between 550 and 590 nm (depending on size and shape of the particle) [84, 85].The controlled and tailored characteristics of synthesized CuO-NPs require the determination of ideal concentration of stabilizing/reducing agents. To understand and quantify the effects of different dosages of stabilizing/reducing agents, the CuO-NPs were synthesized through the reduction of Cu^{2+} to Cu^0 by adjusting the SH concentration from 0.05-0.25% (w/v) while keeping other parameters constant (Fig. 1b). Further, it was observed that no apparent absorption was found between 550 and 590 nm at 0.05%SH inferring no appreciable effect on the reduction of Cu^{2+} ions. However, as the concentration of SH was raised to

0.10%, a reduction peak at 533 nm began to rise, indicating the beginning of reduction process. A strong and sharp peak was exhibited by increasing the SH concentration further to 0.15%. Further, a considerable red shift from 550 to 650 nm was observed, even though the reaction's maximum absorption intensity was obtained at 0.20% SH, which may be due to the increase in the size of the nanoparticles [86]. Also, when SH concentration was increased further to 0.25%, the intensity of the absorption dramatically decreased, resulting in an additional red shift of 610 nm. Here, rather than the interactive effects with saturated Cu^{2+} ions, the increased concentration of SH caused the contact between functional groups. As a result, nanoparticles changed into clusters or CuO-hydro-complexes rather than particles [87]. As a result, the optimal concentration for this reduction process was found to be 0.15% SH.

A suitable amount of reaction incubation time (t) is necessary to reach the yield point of reduction under the conditions of complete nucleation and the resulting stability of CuO-NPs. To regulate the time of equilibrium for particle development and stability, the spectrophotometric investigation of the reaction kinetics of particle formation was performed (Fig. 1c). No obvious peaks were recorded during the first 20 minutes of the reaction, thereby indicative of the absence of CuO-NPs synthesis. A faint and broad peak with little to no absorption intensity was observed at 535 nm after 30 minutes of reaction. Also, there was a notable rise in the intensity of peak absorption and sharpness and strength of the band after another 10 min of reaction time. Although, the reaction increased the absorption intensity over a 50-min time period, the band widened and experienced a considerable red shift to 610 nm, suggesting instability in the formed nanoparticles. The growth and stabilization of CuO-NPs was fully achieved within 40 min of the reaction. It is necessary to carry out the synthesis reaction at an appropriate temperature (T) in order to obtain the specific size/shape of nanoparticles.

As a result, the temperature range between 30-70°C was used for the temperature-dependent synthesis of CuO-NPs (Fig. 1d). The reaction was conducted between 30 and 70°C and a strong noticeable absorption band was seen at 50°C confirming the formation of CuO-NPs. The results exhibited a negative association between temperature and particle size, with further increase at 70°C showing no increase in absorption intensity or sharpening of absorption band but causing disappearance and widening of absorption peak [52, 88]. The optimized temperature for the production of SH assisted CuO-NPs was found to be 50°C. Also, the pH of the reaction also plays an imperative role in the control of growth and properties of synthesized nanoparticles. The biosynthesis of SH-CuONPs was undertaken at variable pH (4–12) (Fig. 1e). The pH-dependent wavelength absorptive spectra exhibited no promising visible peaks at both acidic (pH = 4–6) and basic (pH = 10–12). However, the reduction of Cu^{2+} ions and subsequent production of CuO-NPs were indicated by a distinct and strong absorption peak at near neutral to slight basic pH 8. A broad absorption band and steady absorption intensity were the consequences of the reaction under both acidic and basic extremities of the reaction media.

The nanoparticles mediated biological activities, particularly their antimicrobial effects, are influenced by a number of factors, including their surface charge, capping agent, ionic strength, pH, size morphology and shape [89]. The functionality of metal nanoparticles for different applications is further enhanced by adjusting their size and shape. During the optimization of synthetic procedures of nanoparticles by biological pathway, the precise control of these parameters may be crucial. By altering the medium's pH, it is possible to influence the shape and size of nanoparticles, with an acid pH resulting in the generation of large NPs. This is because there are more functional groups available at higher pH ranges than at lower pH ranges, making them

559 more accessible for nucleation [90]. Besides pH, the solution concentration also
560 influences the size and form of biosynthesized nanoparticles. A quick change in the
561 color of the reaction mixture is the primary indicator that the reaction's time is
562 important in the reduction of nanoparticles and their size. This time frame can
563 range from minutes to hours. The shape, size, and yield of nanoparticles are also
564 influenced by the reaction temperature, which is another crucial factor in the
565 biosynthesis of nanoparticles [89].

566 Polysaccharides are essential compounds for the creation of multi-facet nano-
567 based materials since they serve as the foundation for fibers, coatings, and stabilizing
568 agents [91]. They are renewable resources that have undergone extensive research
569 owing to their biodegradability, biocompatibility, and variety of biological activity [92,
570 93]. They are organic macromolecules made up of covalently bonded monosaccharide
571 units connected by polymer chains [94]. Today, a multitude of polysaccharides are
572 obtained through extraction from natural sources such as microorganisms, algae, plants,
573 animals [95]. The mechanism of formation of polysaccharides units (here, hyaluronate;
574 Fig. 2) assisted metal based nanoparticles (here, CuO-NPs) can be explained as follows:
575 Metal ions are hosted by the units of polysaccharides by non-covalent bonding
576 (sorption). By changing the order of free energy (heating), the metallic precursor is
577 subsequently reduced to a zero-valent state, initiating the process of nucleation and
578 formation of nanocrystal. The metal nanoparticles are stabilized by the rise in
579 temperature, which also enables control over their growth kinetics and shape. In
580 contrast to top-down synthesis, when the initial materials are shrunk down through
581 chemical, thermal, or mechanical processes, this sort of self-assembling (bottom-up)
582 synthetic process is favored. These processes could cause the nanoparticles to oxidize
583 unintentionally, changing their surface chemistry and/or physical characteristics.

584 Furthermore, sans an external stimulation like a pH shift, the stabilized metal based
585 nanoparticles do not readily leach out of the integrated metal ion-
586 polysaccharide complex. Since most polysaccharides are sensitive to pH changes, they
587 are frequently used in polysaccharide-based systems for controlled drug delivery [96,
588 97].

589

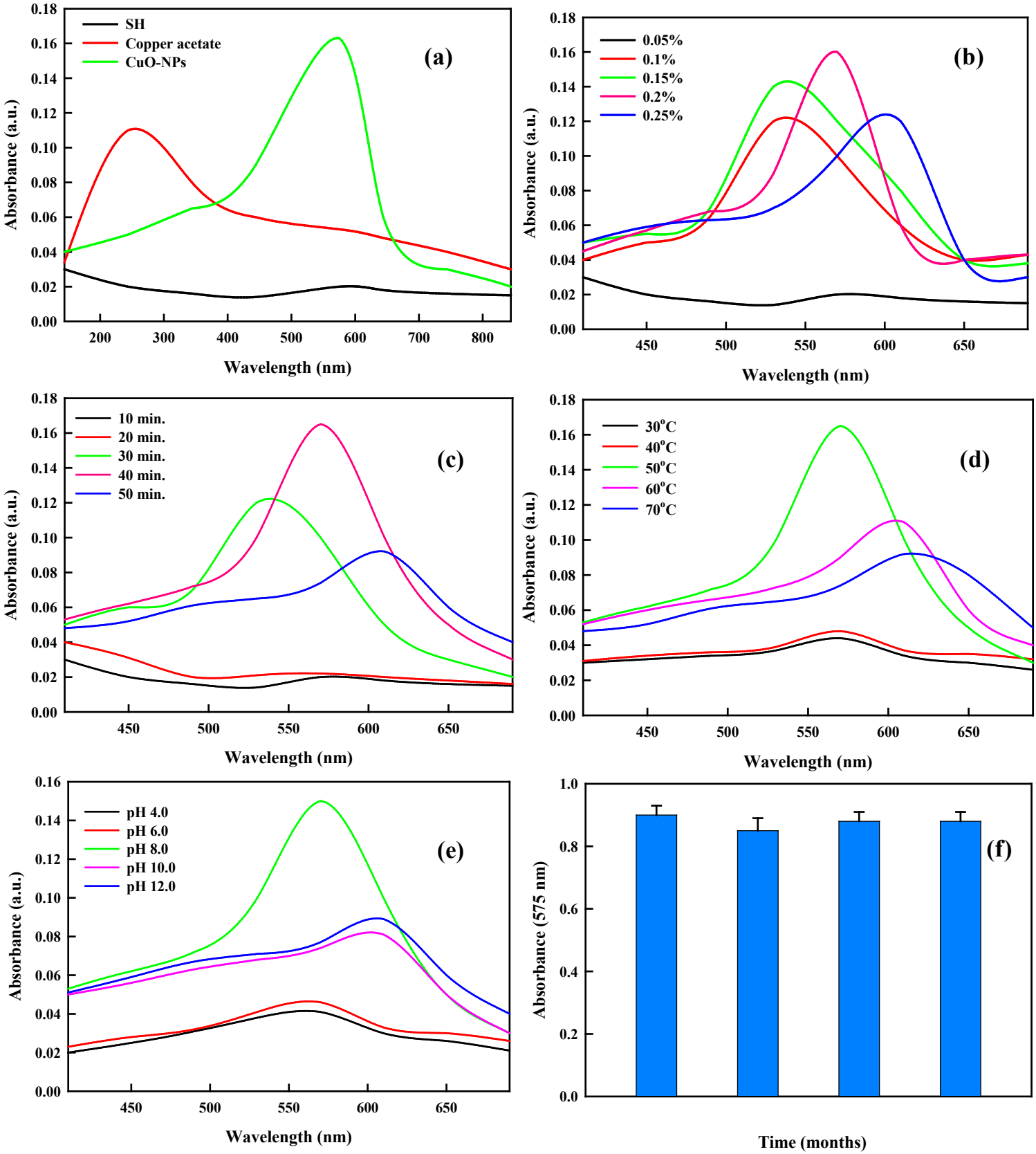

590 **Fig.1** (a) UV–Vis spectra of SH, copper acetate and CuO-NPs. Effect of (b) SH concentration, (c)
591 reaction time, (d) reaction temperature, (e) pH, (f) stability over time

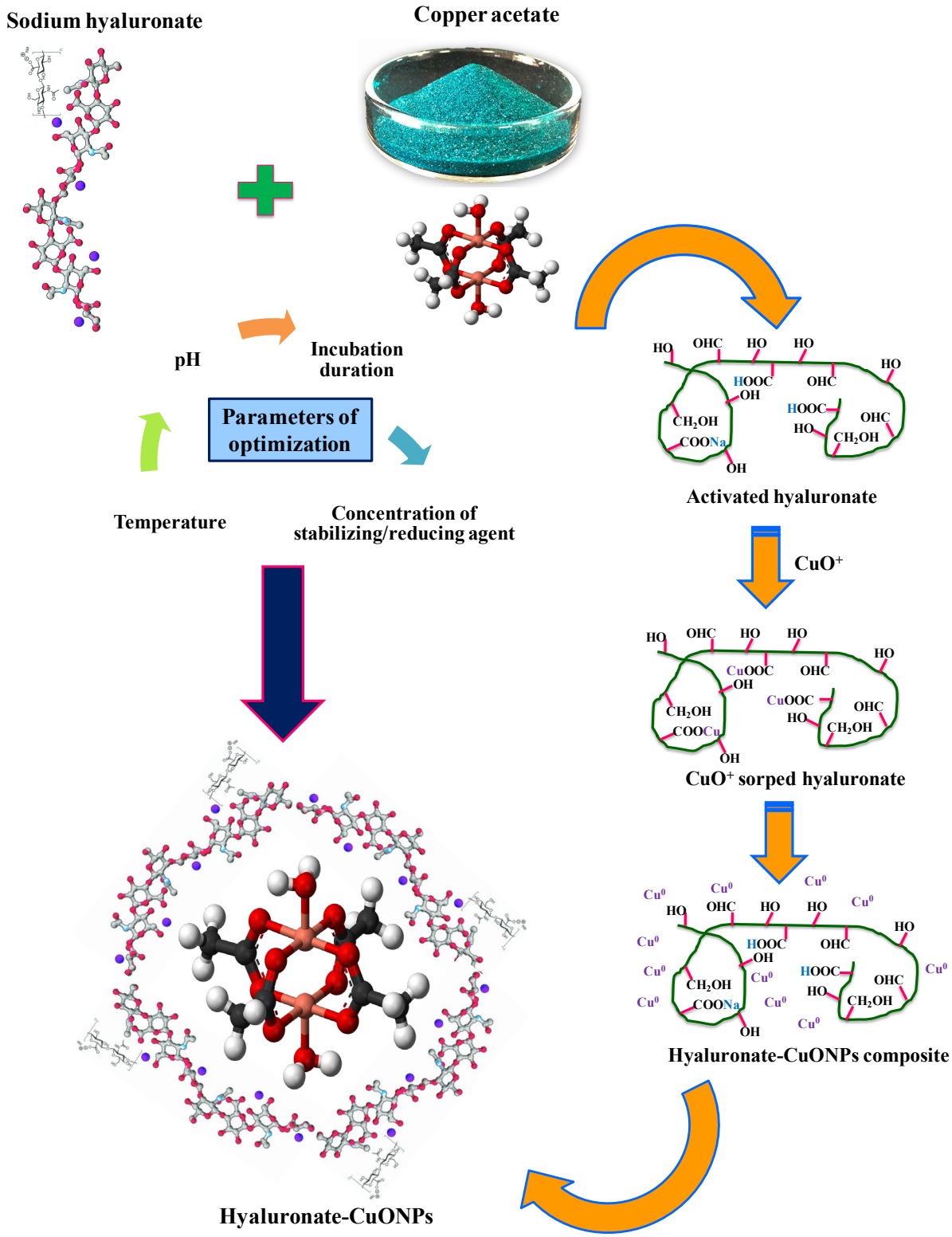

Fig. 2 Mechanism of hyaluronate assisted CuO-NPs synthesis

3.2. Characterization of fabricated CuO-NPs

For the biosynthesis of SH assisted CuO-NPs in the current investigation, a matrix of sodium hyaluronate was used. After washing, drying, and annealing, a fine black powder of CuO-NPs was produced, and stored till further processing for morphological, physiochemical, and biological experimentations. The initial TEM analysis of the morphology and size of CuO-NPs exhibited successful synthesis of polydispersed CuO-NPs with a particle size of 17.4±1.3 nm (Fig. 3a and b). The observation also demonstrated the oval and spherical form of SH-produced CuO-NPs. The high-resolution TEM was used to capture a section of a single particle, demonstrating highly crystalline surface of CuO-NPs. Additionally, SEM was used to observe the solid-state particles (Fig. 3c). It revealed that CuO-NPs was equally distributed throughout the SH composite with no aggregation, demonstrating the ensnarement of CuO-NPs in SH molecules conferring stability. Furthermore, the EDX microanalysis showed the presence of copper component (29.49%) in nano form rather than copper derived compounds (Fig. 3d). The purity and structural morphology of CuO-NPs was shown by X-ray diffraction pattern found with diffraction angles ranging from 10 to 70. Strong peaks at 23.44, 31.18, 34.38, 37.58, 38.80, 43.60, 47.65, 57.24, 60.43, 65.11 and 66.95 corresponding to the miller indices (100), (-111), (002), (-102), (-211), (-112), (012), (-221), (020), (-312) and (021) confirmed with JCPDS file no. 048-1548 [98] (Fig. 4a). The Debye Scherrer equation exhibited the crystalline monoclinic phase of CuO-NPs. Similar results were also reported in the studies of [3, 57, 99, 100]. It was important to note that the crystal size calculated by the XRD using the Scherrer equation (16.67 nm) was relatively smaller than the particle size discovered in TEM (17.4±1.3 nm). The size of twinned particles with multiple diffraction domains is lower

than the diameter measured by XRD analysis, which is a measure of single-crystal particles and could be the cause of the size discrepancy. The TEM image (Fig. 2b) substantiated the theory and clearly demonstrated that some particles were >16 nm with grain twinning and boundary [101].

The FTIR chemical analysis was used to understand the interaction between SH and copper oxide ions (Fig. 4b). The primary peaks of aqueous SH identified were: 3370 cm^{-1} (-OH stretch), 1412 cm^{-1} (C-H stretch), and 1082 cm^{-1} (C–O–C). The CuO-NPs had comparable spectral morphologies, but their peak positions had a tiny shift to the lower bands (3579, 3482, and 1120 cm^{-1}, respectively) as a result of conformational changes that were caused by CuO-NPs in SH chains through dipole-dipole interactions and H-bonding. Also, a prominent SH peak (indicated by a rectangular area) at 1405 cm^{-1} (C-O-C) was totally absent, while the peak at 1157 cm^{-1} sharpened as a result of the vibrational stretch of (NH)C==O. Therefore, it is clear that the interaction between functional groups of SH, particularly-OH,-NH(C)=O, -COOH groups, and CuO-NPs enabled reduction of Cu^{2+} ion. These interactions were suggestive of the SH macromolecule capping and stabilizing CuO-NPs.

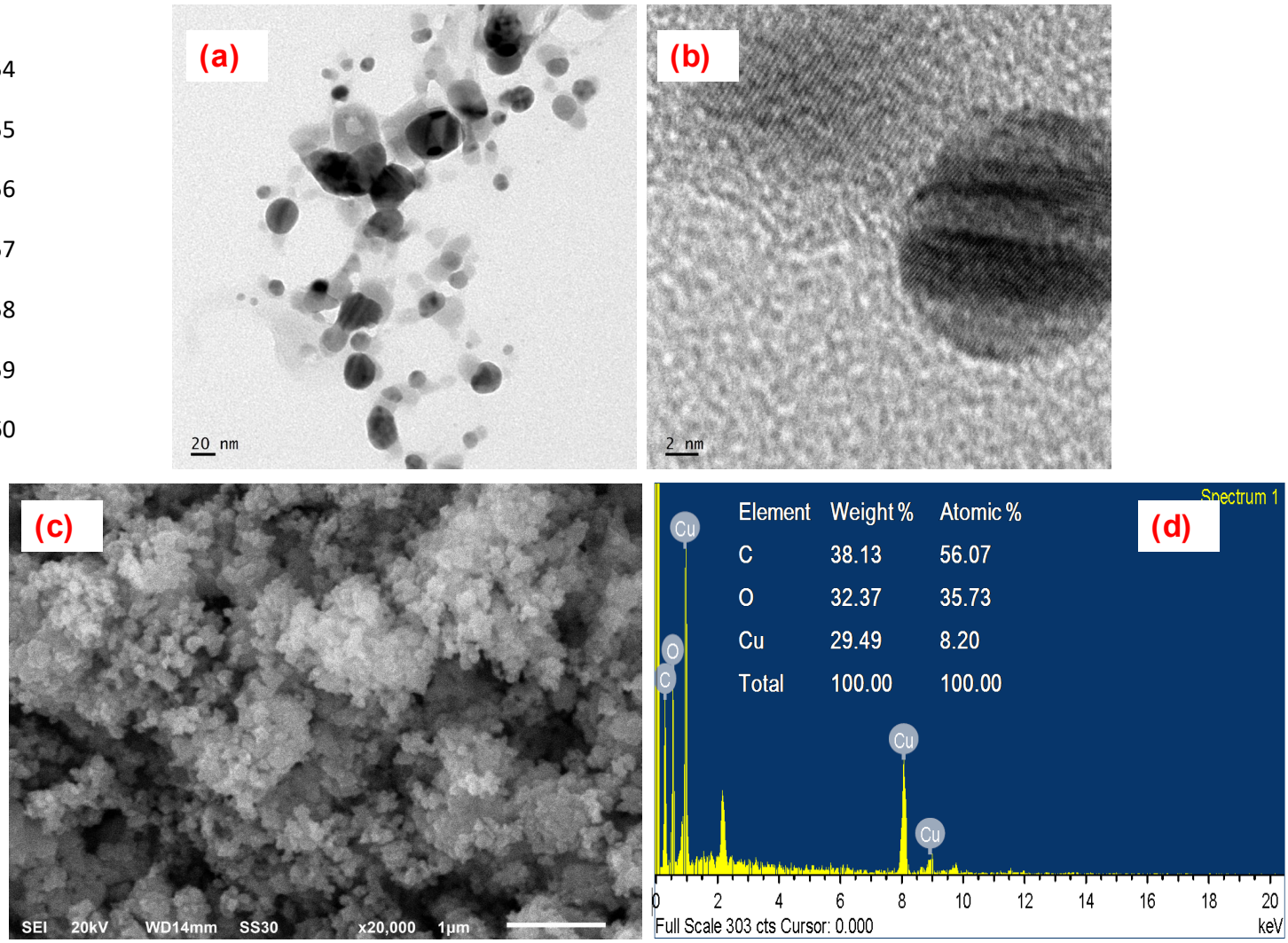

Fig.2 Electron microscopic analyses of CuONPs. (A) TEM image at 20 nm; (B) TEM image at 2 nm; (C) SEM micrograph at 20000X and (D) EDS spectrum displays the % of C, O and Cu elements in SH-CuONPs.

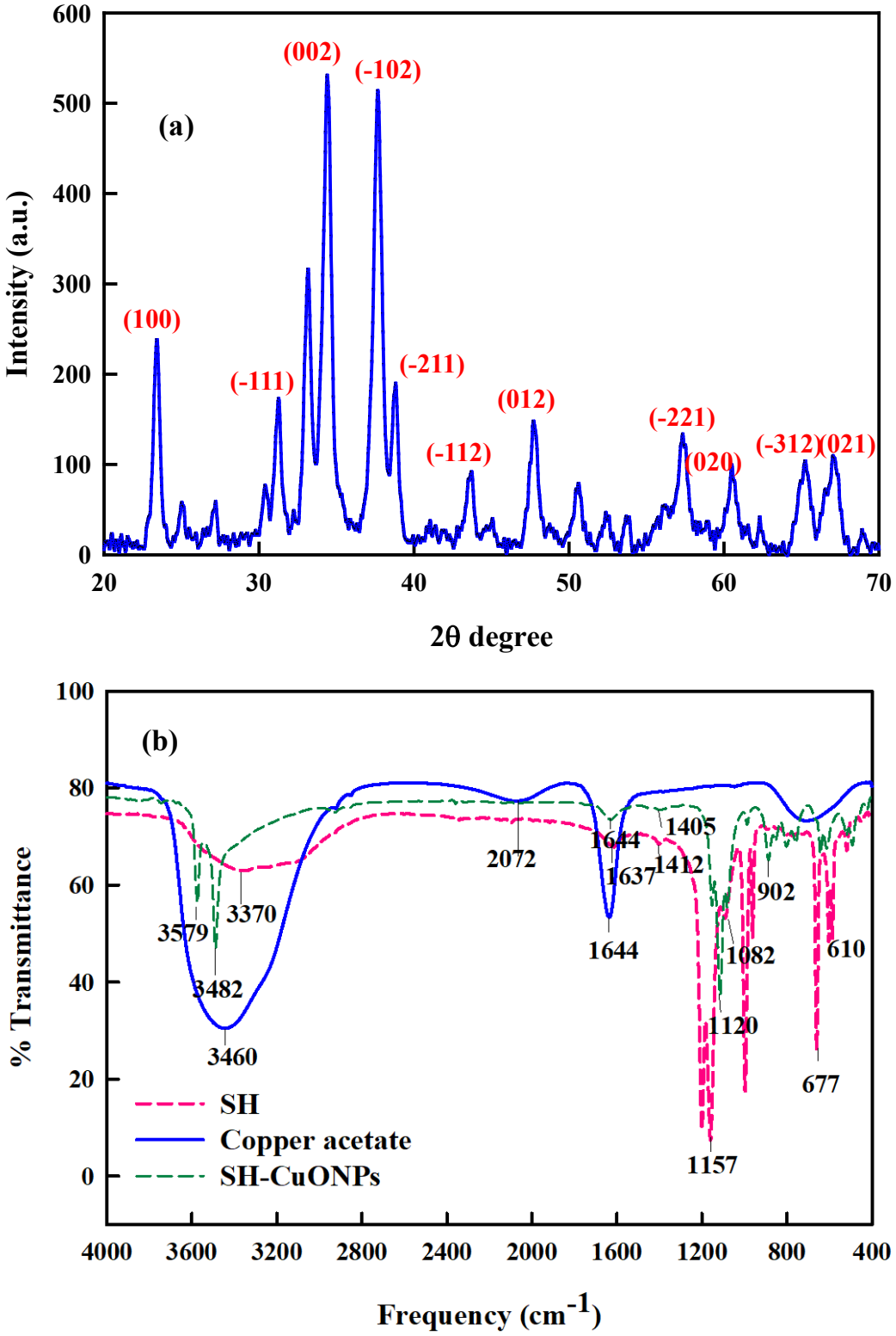

Fig.3 Physicochemical characterization of CuONPs. (a) X-ray diffraction (XRD) (b) FTIR analysis

685

686 **3.3. Biological activities of CuO-NPs**

687 Diabetes and its complications are a severe and common source of illness and
688 mortality all over the world. A metabolic disease known as diabetes melitus (DM) is
689 characterized by chronic hyperglycemia induced by cellular insensitivity to insulin or
690 decreased insulin production [102]. Some phyto-based chemicals have been reported as
691 inhibitors of starch hydrolysis and are considered an appealing contender in the
692 treatment of diabetes mellitus in addition to anti-diabetic medications used in the
693 regulation of post-prandial hyperglycaemia. To assess the ability of SH assisted CuO-
694 NPs in the inhibition of enzyme α-amylase; the former was subjected to experimental
695 assay. The results revealed that biosynthesized CuO-NPs showed a satisfactorily high
696 amount of α-amylase and α-glucosidase enzyme inhibitions (72±1.2% and 70±2.1%), as
697 compared to that of SH at 100 μg/ml (Fig. 5a, b). According to our findings, the SH
698 assisted CuO-NPs exhibited significant enzymatic inhibitory activity which were
699 similar to the reports of [43, 100, 103]. Also, the graphic representation of HbA1c assay
700 results (Fig. 5c) inferred a dose-dependent inhibition. It was clearly explained as a
701 concentration-dependent reduction in the % of inhibition at various concentrations of
702 biosynthesized CuO-NPs (20-100 μg/ml). The maximum concentration (100 μg/ml) of
703 CuO-NPs and metformin, exhibited maximum inhibitions of 70±2.1% and 86±1.4%,
704 respectively, whereas the minimum concentration (20 μg/ml) of CuO-NPs and
705 metformin exhibited the least inhibitory value. There are a number of causes for α-
706 amylase inhibitory potential of medicinal plants, such as concentration of fibre, fibre
707 cocooned encapsulation of enzyme and starch, and inhibitors on fibre surface, resulting
708 in the reliable adsorption of enzyme α-amylase onto the surface of fibre and reduced
709 starch accessibility to enzyme, resulting in the diminished activity of α-amylase [104].

By delaying carbohydrate digestion and lengthening the overall time of carbohydrate digestion, α-glycosidase inhibitors can aid in lowering post-meal blood sugar levels. The inhibitors such as miglitol, vogomibose, and acarbose have been utilized as first-line therapies for diabetes type 2 in the clinical context. Unfortunately, these therapies may have unwanted consequences like bloating, stomach pain, and diarrhea. Therefore, for the proper management of diabetic diseases, the development of safe and efficient enzyme inhibitors is necessary [105, 106].

A biologically active enzyme called urease breakdown urea into carbon dioxide and ammonia. Urea is widely distributed in biologically active soil because many microorganisms metabolize it through the enzymatic action of urease [107]. The SH-assisted CuO-NPs displayed outstanding urease inhibitory potential, as evidenced by the urease inhibitory assay results, which showed % inhibition of 68±2.1% compared to thiourea at 100μg/ml (Fig. 5d). During biosynthetic process, the functional groups attached to CuO-NPs may be responsible for this inhibitory action. Further, the triglycerides are hydrolyzed into fatty acids and glycerol molecules by a class of enzymes called lipases. These fat-splitting enzymes can be found in the pancreatic secretions, stomach juices, and blood [108]. In the present study, SH-assisted CuO-NPs exhibited high potential for inhibiting enzymatic activity of enzyme lipases. At 100 μg/ml, CuO-NPs demonstrated a percent inhibition of 70±2.3% (Fig. 5e). The biological molecules conjugated to CuO-NPs during the biosynthesis process may be a plausible factor contributing in the inhibitory effect. This inhibitory property may be brought on by the various biological molecular species and functional groups like -OH (hydroxyl) and C=O (carbonyl) groups [107, 109].

Free radicals are molecules devoid of full electron shell, which speeds up a chemical process compared to other molecules. Oxygen (O_2) is the most significant free radical in physiological systems. Radiation causes O_2 to transfer electrons from other molecules, causing the destruction of DNA and other molecules [110-112]. Some of these modifications lead to illness such as cancer, diabetes, heart issues, and muscle failure. Antioxidants sweep away free radicals like a broom, repairing damaged cells as demonstrated by the studies of [113, 114]. The antioxidant assays of FRAS, TRP, TAC, FRAP, and ABTS are used to examine the antioxidant capacity of CuO-NPs. The FRAS assay was analyzed by using DPPH molecule. The colour of the stable free radical DPPH is purple with a significant absorption maximum observable at 517 nm. The free radical in the DPPH is paired off in the presence of an antioxidant, which reduces the absorbance and colour intensity. The DPPH technique is quick, easy, and affordable to test the antioxidant properties of compounds and is frequently used to assess their capacity to function as hydrogen providers and free-radical scavengers. The DPPH test depends on DPPH, a stabilized free radical, being eliminated. In fact, DPPH is a stable free-radical molecule that has a dark colour and crystalline structure. It is a widely recognized antioxidant and radical test in which the DPPH radical initially exhibits a dark purple tint in solution; however, after reduction and transformation into DPPH-H, it becomes colorless or light yellow [115]. The CuO-NPs reduces DPPH radicals by the transference of an electron or proton. In present study, the amount of DPPH-scavenging activity rose linearly from 20-100 μg/ml of CuO-NPs concentration, exhibiting 70±2.3% scavenging activity at 100 μg/ml (Fig. 6a). The CuO-NPs exhibited a high TAC value of 85±0.26 μg AAE/mg (Fig. 6b). The TRP value of CuO-NPs is larger than that of hylauronate solution at 76±0.35 μg AAE/mg (Fig. 6c). Additionally, the synthesized CuO-NPs had a high ABTS value (400 μM TEAC) and a high FRAP value (423 μM

TEAC) (Fig. 6d and e). Further, the transition metal ions, particularly Fe^{2+}, can hasten lipid peroxidation by (i) initiating fenton reaction or (ii) by breaking down lipid hydroperoxide into alkoxyl and peroxyl radicals triggering a chain reaction. In the study, the treatment of CuO-NPs resulted in an increase of 33% in the metal chelation (Fig. 6f).

The H_2O_2 scavenging capacity of CuO-NPs was experimentally examined. Since, the hydroxyl radical may harm a variety of molecules, including proteins, DNA, lipids, and other highly reactive free radicals, it has been exploited as a highly destructive species in free radical pathology [116, 117]. The findings of the current investigation demonstrated that CuO-NPs had a greater potential for scavenging power with increase in respective NPs concentrations (Fig. 7a). According to reports, CuO-NPs can produce hydroxyl radicals when H_2O_2 is present. The capacity of CuO-NPs to scavenge free radicals may be attributed to the presence of a number of biological constituents with the ability to donate hydrogen atoms in their -OH groups. Also, the nitric oxide scavenging activity of CuO-NPs increased with increasing concentrations of CuO-NPs (Fig. 7b). From the aforementioned findings, it can be inferred that the biomolecules adsorbed on CuO-NPs with antioxidant capacity may have contributed to the reduction and stabilization of CuO-NPs during the synthetic process, hence increasing the antioxidant activity of biosynthesized CuO-NPs. Similar results were also reported by [1, 104, 118]. The reactive oxygen species can oxidize cell membranes, harm membrane proteins, and alter DNA, which can lead to the beginning or worsening of a variety of illnesses. Although, the body has a defense mechanism, ongoing contact with chemicals and other contaminants can increase the amount of free radicals that the physiological system of body cannot neutralize leading to irreparable oxidative damage [119-121]. In order to prevent or treat oxidation-related disorders or free radicals, antioxidants with

783 the ability to neutralize free radicals are crucial. A focused strategy to the biochemical
784 preclusion of malignancies aimed at halt/return cellular system to their pre-cancerous
785 condition without the use of hazardous doses through foods and medications has to be
786 developed as a result of broad molecular cell level investigations on cancer cells [120,
787 122].

788 The peroxidase (POD) activity assay was used to analyze the capacity of SH-
789 assisted CuO-NPs in the degradation of hydrogen peroxide (H_2O_2). Both plants and
790 animals contain large amounts of enzyme peroxidases which catalyzes the oxidation of
791 several phenols and non-phenols derived substances by breaking down H_2O_2. The
792 biosynthesized SH-CuO-NPs were found to be proficient biocatalysts exhibiting a
793 catalytic activity of 0.59 mM/min/mg in comparison to SH solution (0.05 mM/min/mg)
794 (Fig. 7c). Our findings were consistent with the earlier research, which reported that
795 CuO-NPs have peroxidase-like catalytic activity by the production of a blue-colored
796 product post nanoparticles addition to the TMB containing medium as a peroxidase
797 substrate [44, 100]. So, SH-assisted CuO-NPs are an excellent choice as peroxidase
798 mimics for a variety of possible applications due to their catalytic properties. The
799 metabolic process in mitochondria produces ROS and RNS as a byproduct. The DHR
800 123 probe was used to assess the amount of ROS/RNS. According to the findings shown
801 in Fig. 7d, the CuO-NPs generated more ROS and RNS in yeast cells than the control.
802 The CuO-NPs were found to generate up to 3400 ROS/RNS when incubated with yeast
803 cells, compared with control (610 ROS/RNS). In general, mitochondrial respiration
804 produces free radicals, with electron transport chain (ETC) serving as the site of ROS
805 production and oxygen leakage. The relevance of metallic nanoparticles improved the
806 ability of fenton reaction in the production of free radicals. Additionally, the metallic
807 ions in nanoparticles can prevent mitochondrial electron transport, increasing the

808 formation of ROS. Similar outcomes were noted in earlier studies where the use of
809 metal derived nanoparticles led to ROS generation [123]. The cellular mechanism was
810 severely compromised due to the increased levels of ROS/RNS caused by an imbalance
811 between the free radicals and their scavenging activity.
812

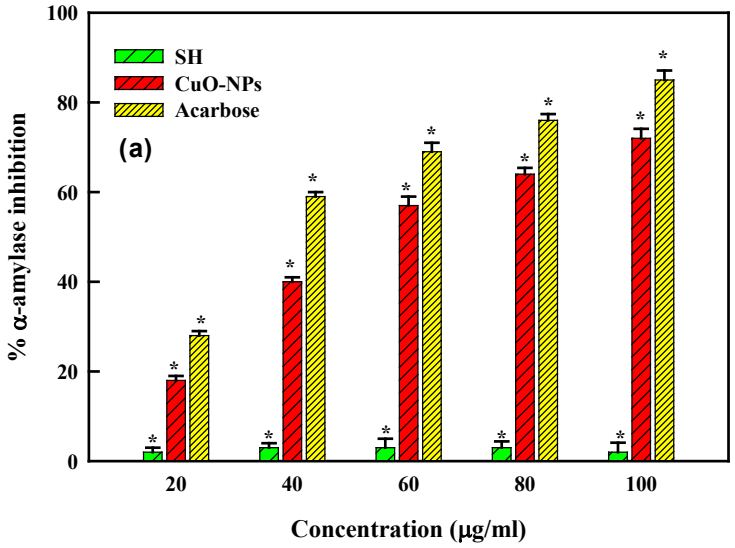
SH
CuO-NPs
Acarbose
(a)
% α-amylase inhibition
Concentration (µg/ml)

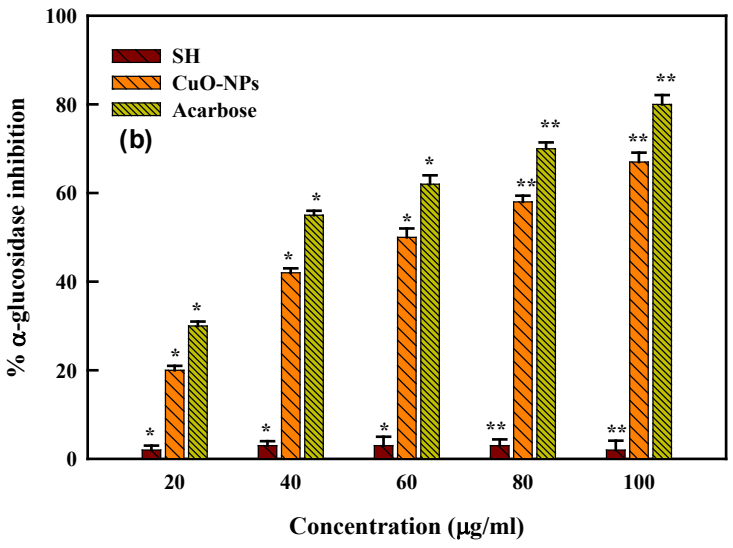
SH
CuO-NPs
Acarbose
(b)
% α-glucosidase inhibition
Concentration (µg/ml)

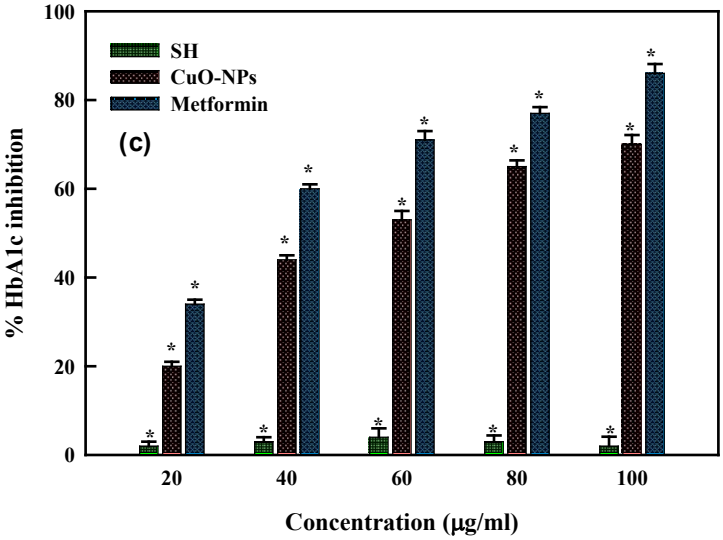
SH
CuO-NPs
Metformin
(c)
% HbA1c inhibition
Concentration (µg/ml)

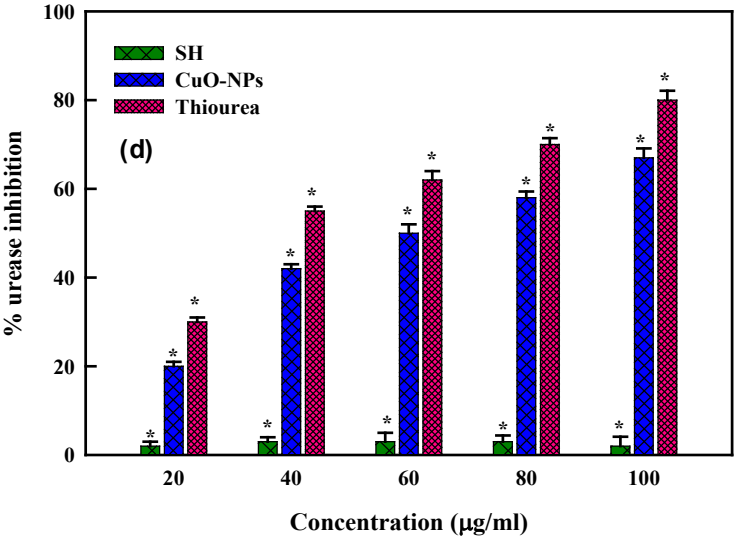
SH
CuO-NPs
Thiourea
(d)
% urease inhibition
Concentration (µg/ml)

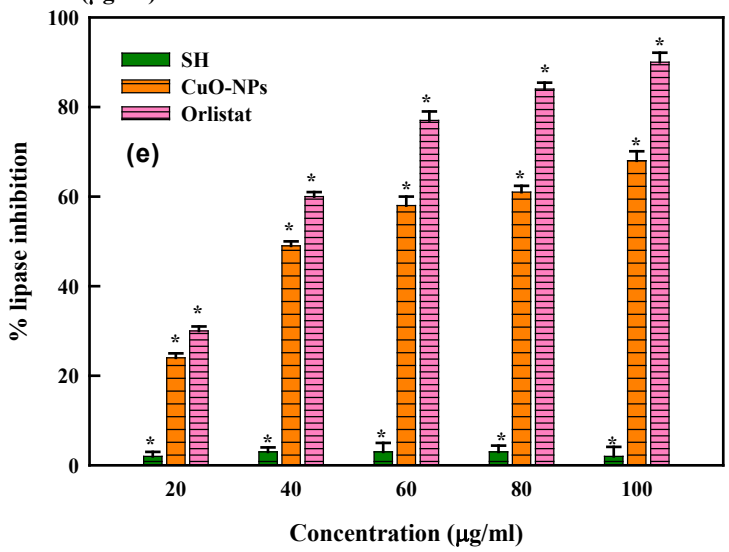
SH
CuO-NPs
Orlistat
(e)
% lipase inhibition
Concentration (µg/ml)

820

821

822 **Fig. 5** Biological activity of CuO-NPs. (a) α-amylase, (b) α-glucosidase, (c) HbA1c,(d) urease and
823 (e) lipase inhibitory activities.

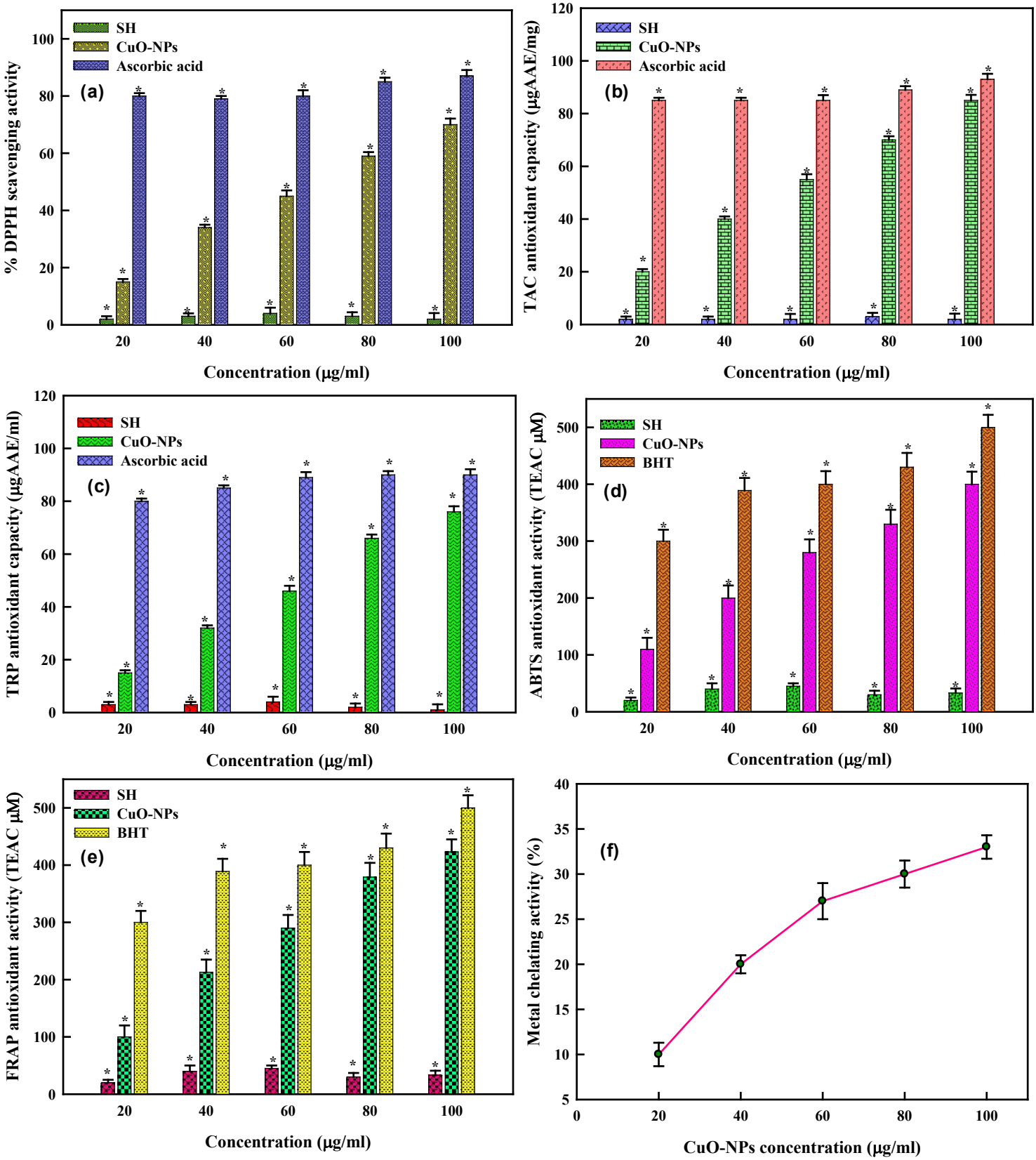

824 **Fig. 6** Antioxidant activity of CuO-NPs. (a) DPPH, (b) TAC, (c) TRP, (d) ABTS, (e) FRAP and (f)
825 metal chelation activities.

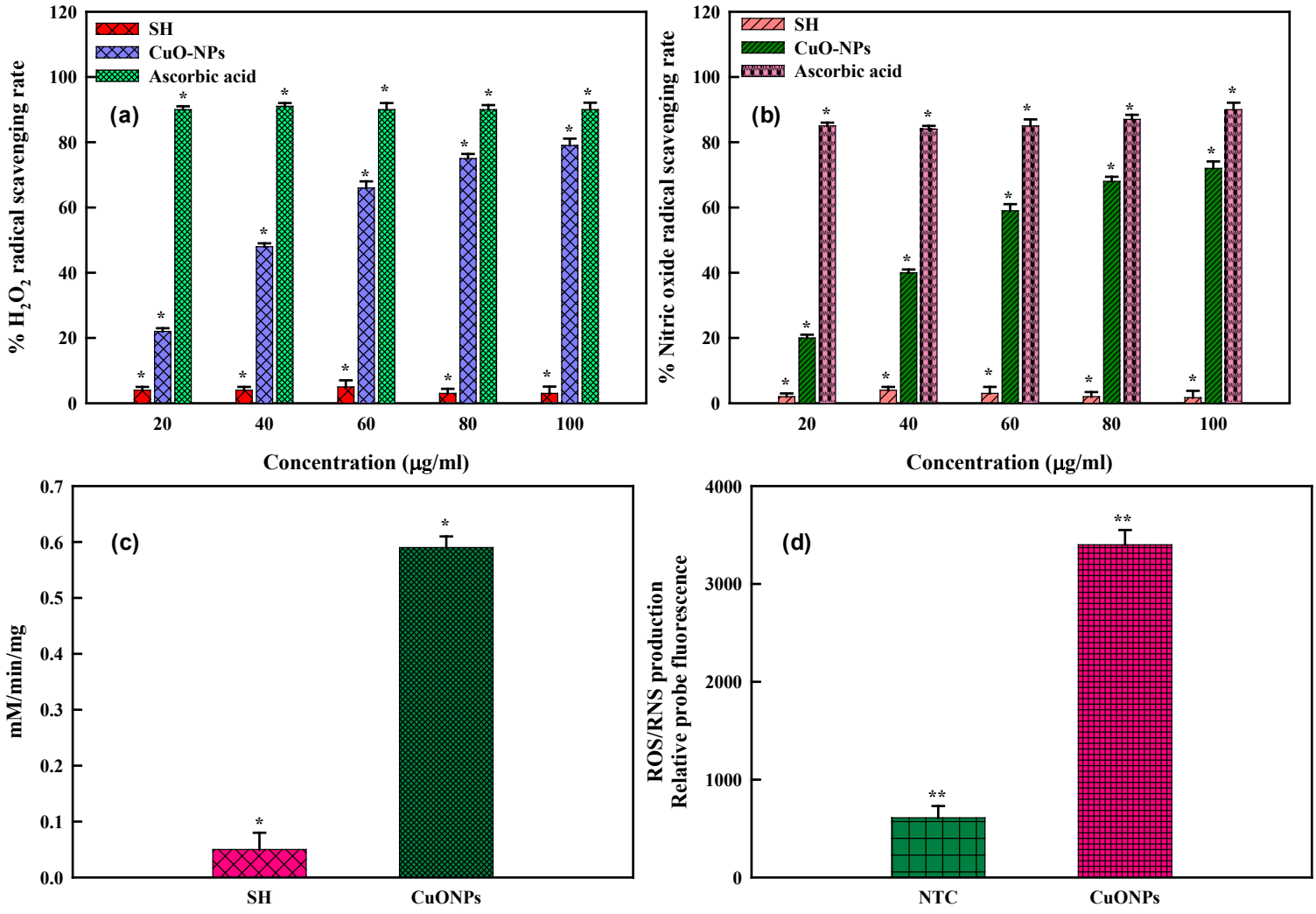

826 **Fig. 7** Antioxidant activities of CuO-NPs. (a) H_2O_2 radical scavenging activity, (b) NO_2 radical
827 scavenging activity, (c) peroxidase-like catalytic activity, (d) ROS/RNS measurement (NTC=non
828 treated cells).

829 Antibiotic resistance is one of the most serious public health problems, which is
830 caused by inappropriate or excessive use of antibiotics [1, 3, 124, 125]. The urgent need
831 to develop new antibiotic agents, use active and widespread techniques of infection
832 control to stop the development of antibiotic resistant strains, and prolong treatment
833 including hospitalization and recovery all contribute to increased healthcare costs. The
834 occurrence of fatal and hazardous adverse effects from utilizing antibiotics in treatment,

such as anaphylactic shock (or hypersensitivity reactions), growth suppression of hematopoietic stem cells, and liver and kidney failure in some patients, are the additional issues. Even while only a small number of patients may experience these consequences, they are nonetheless significant because they can be fatal and harmful. The use of nanoparticles in medicine and related fields has grown significantly as a result of the development of nanotechnology science and the discovery of their antibacterial characteristics [126]. Also, the resistance of many infections to antibiotics is one of the primary issues facing medical science, the potential antibacterial actions of biosynthesized nanoparticles are crucial. In current study, the agar well diffusion technique was used to assess the antibacterial efficacy of green produced SH-assisted CuO-NPs against both gram +ve and gram-ve pathogenic bacteria (Fig. 8a). The tested bacterial strains were effectively inhibited by CuO-NPs with the maximal zone of inhibition reported in *E. coli* (27 mm) followed by *S. aureus* (22 mm). No inhibition was reported in negative control setup. Also, the cellular leakage of biological molecules like proteins and nucleic acids increased with successive increase in CuO-NPs concentrations (Fig. 8b and c). The *E. coli* cells exhibited higher levels of protein leakage (112 μg/ml) than *S. aureus* (78 μg/ml) post 6h time treatment. Similar results were also observed in nucleic acid leakage in which *E.coli* cells (0.2 OD_{260}) leaked more amounts of nucleic acids than *S. aureus* (0.11 OD_{260}) post 6h treatment. Both intracellular and extracellular interactions may be responsible for the antibacterial activity of CuO-NPs against human pathogenic organisms [127, 128]. The potential interaction between the CuO-NPs and the outer bacterial membrane may be due to growth suppression by the former. CuO-NPs have the potential to compromise bacterial cell viability by impairing enzyme performance and increasing cell permeability [129, 130]. CuO-NPs may also integrate within cell membrane owing to their small size compared to the membranal

pores on bacterial cell surface. Additionally, CuO-NPs produce reactive oxygen species like hydroxyl and superoxide free radicals, which harm cells by oxidizing double bonding of phospholipids and disrupting membrane permeability, leading to high osmotic stress and finally leading to bacterial cell death [131, 132] (Fig. 9).

An urgent necessity exists to investigate novel approaches to treat infections and diseases linked to bacterial biofilm as a result of the emergence of MDRB (multi drug resistant bacteria) based biofilm-associated infections. The contents of bacterial biofilm based on constitutive components are broadly classified into: hydrophobic (lipopolysaccharides, lipids, surfactants) and hydrophilic (proteins, nucleic acids, polysaccharides) [133]. The anti-biofilm action of nanoparticles (NPs) is significantly influenced by a number of factors, like charge, size distribution, hydrophobicity, surface chemistry, etc. The NPs interact and penetrate biofilm compartments when positioned adjacent to the biofilm [134]. In this study, the biofilm inhibitory potential of CuO-NPs against the cells of *E. coli* and *S. aureus* was evaluated. The CuO-NPs concentrations (20-100 μg/ml) inhibited the formation of biofilm compared to control (Fig. 8d). The CuO-NPs concentrations of 20, 60, 80 and 100μg/ml decreased the biofilm formation (in *E. coli* cells) by 33.1%, 60.02%, 78.4%, 85.32% and (in *S. aureus* cells) by 22.3%, 40.12%, 60.34%, 71.2%, respectively. In agreement with our outcomes, Oliver *et al*. [135] reported 99.9% biofilm reduction at 5 μg/ml AgNPs while no discernible anti-biofilm effect was exhibited by citrate-reduced AgNPs. Strains of *S. aureus* and other biofilm forming bacteria are the principal microbial species responsible for the nosocomial infections linked to catheters. It is demonstrated that catheters coated with metallic nanoparticles significantly inhibit the in-vitro biofilm producing ability of pathogens. Additionally, the consistent release of metallic ions was helpful for patients with invasive devices.

884 The metallic nanoparticles might stop the respiratory enzymes and electron
885 transporters of the pathogens, leading to bacterial death [1].

886 DNA typically interacts with metal complexes in a variety of ways, and these
887 interactions have a significant impact on the structure and function of DNA [136]. They
888 have a strong affinity for DNA and have the ability to cause DNA cleavage [136]. The
889 bio-efficacy of majority of the anticancer medications is frequently correlated with their
890 DNA interaction capacity. Such substances can cause apoptosis and inhibit cell
891 proliferation in cancer cells by destroying their DNA structure [136]. Hence, the ability
892 of SH-assisted CuO-NPs to cleave DNA was evaluated using agarose gel
893 electrophoresis. It is an effective method for identifying DNA damage. DNA is broken
894 at specified sequence areas on the genome during agarose electrophoresis for DNA
895 typing [137]. The transformation of pBR322 DNA form from supercoiled circular
896 conformation (Form I) to nicked circular conformation (Form II) and linear
897 conformation (Form III) serves as a DNA cleavage check. The nuclease activity was
898 visible in all concentrations of CuO-NPs (Fig. 10). Control experiments using pBR322
899 plasmid DNA didn't show any DNA cleavage activity (Lane 1). At 20 μg/ml, the
900 supercoiled plasmid DNA was transformed into circular shape. However, at greater
901 concentrations (60 and 100μg/ml), Form I was transformed into more dense Form III.
902 Based on the results, SH-assisted CuO-NPs served as a powerful chemical nuclease for
903 the breaking of double strand DNA; demonstrating their potential as a DNA target
904 agent and an alternative cancer treatment. Similar reports were reported by the studies
905 of [1, 136-138].

906
907

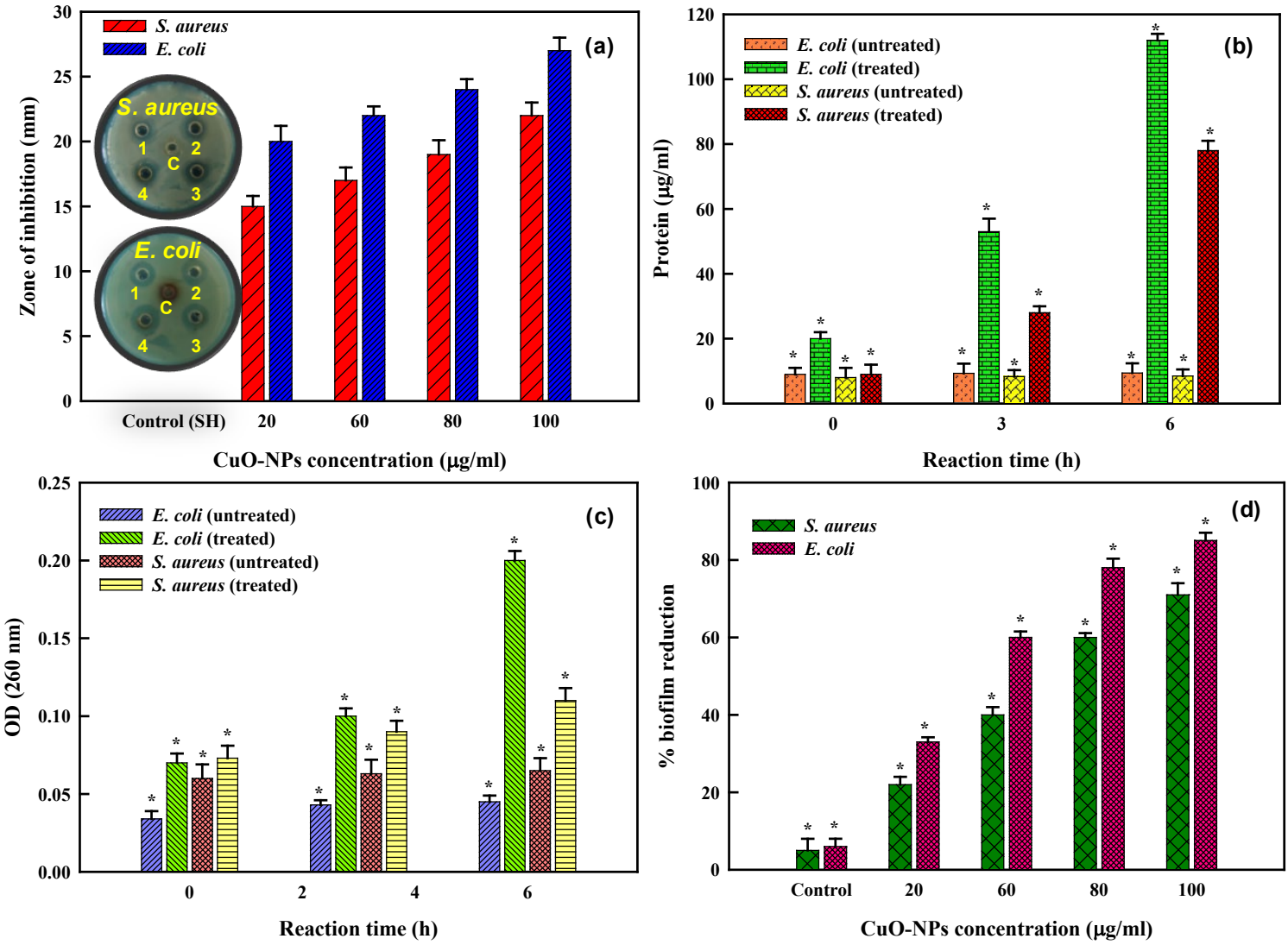

908 **Fig. 8** Antibacterial activity of CuO-NPs (a) well diffusion assay, (b) protein leakage, (c) nucleic
909 acid leakage, and (d) antibiofilm activity.
910
911

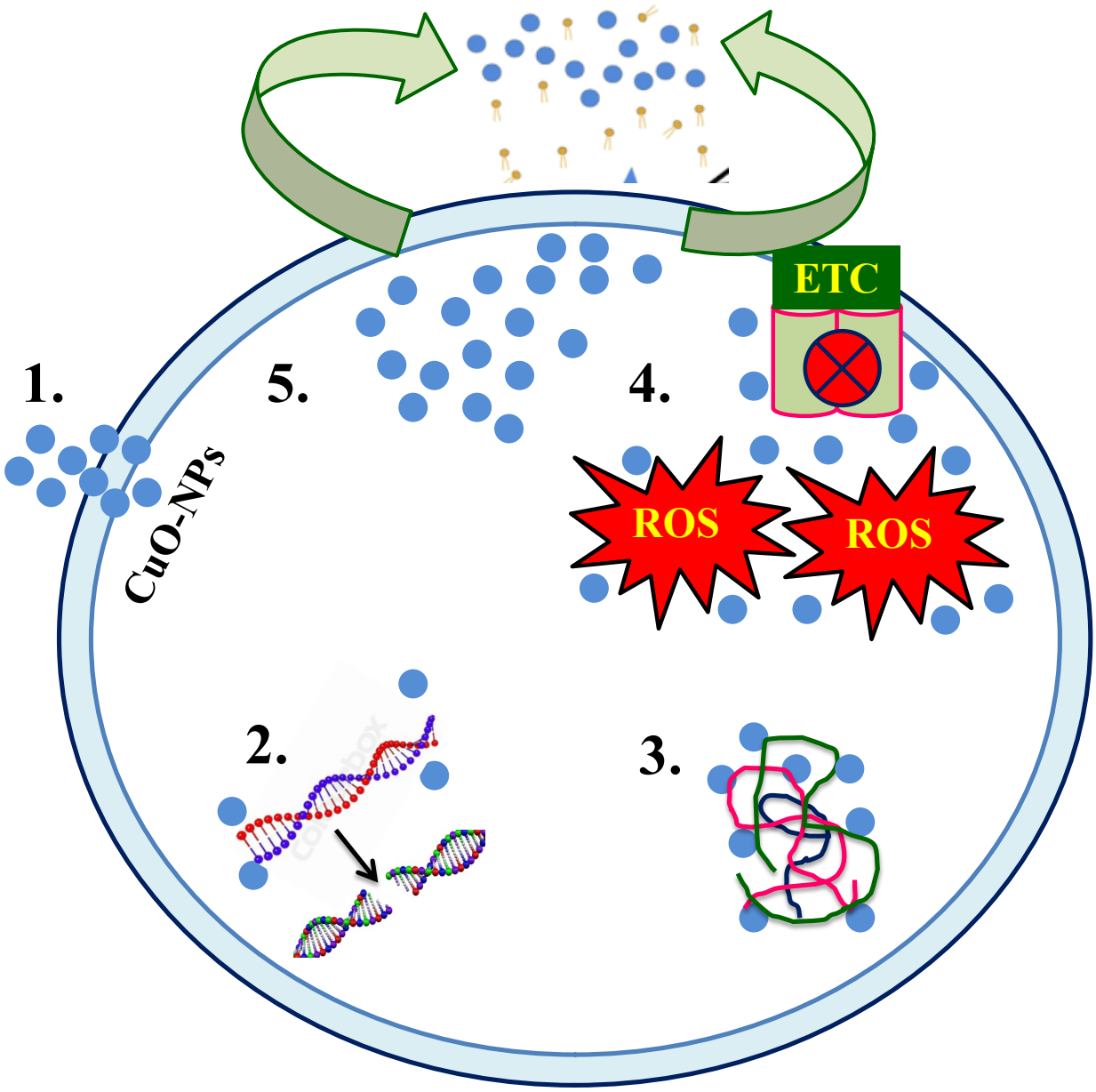

Fig. 9 Mechanism of antibacterial activity of CuO-NPs.
1. Interaction of CuO-NPs with cellular membrane; leading to decreased transmembrane electrochemical potential affecting membrane integrity.
2. DNA damage due to interaction with CuO-NPs.
3. Interaction of Cu^{2+} ions with sulfhydryl groups of proteins.

4. Entry of CuO-NPs and Cu^{2+} ions inside cell; creating oxidative stress which leads to cell death.

5. Accumulation of CuO-NPs on cell surface leaking to cell leakage.

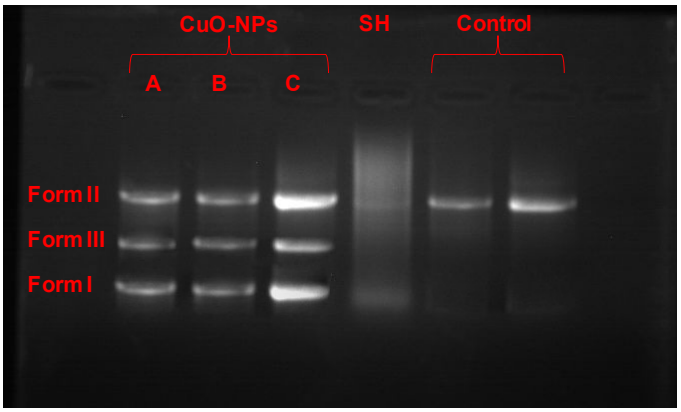

Fig. 10 Cleavage patterns with various concentrations of CuO-NPs.(A) 20 µg/ml, (B) 60 µg/ml, (C) 100 µg/ml, Control= pBR622.

The brine shrimp (*Artemia*) is a common model organism used in the toxicological experiments and is a useful substitute in assessing the effects of marine toxicity. In present work, the cytotoxicity of CuO-NPs was investigated on brine shrimp nauplii at different concentrations (20-100 µg/ml) (Fig. 11). The results exhibited that the viability of nauplii decreased in a concentration-dependent pattern; from 95% (20 µg/ml) to 50% (100 µg/ml) which can be ascribed to the effects exerted by the higher concentrations of CuO-NPs. The effects of CuO-NPs were found to be statistically significant ($p < 0.001$). Similar results were also reported by the studies of [139-140]

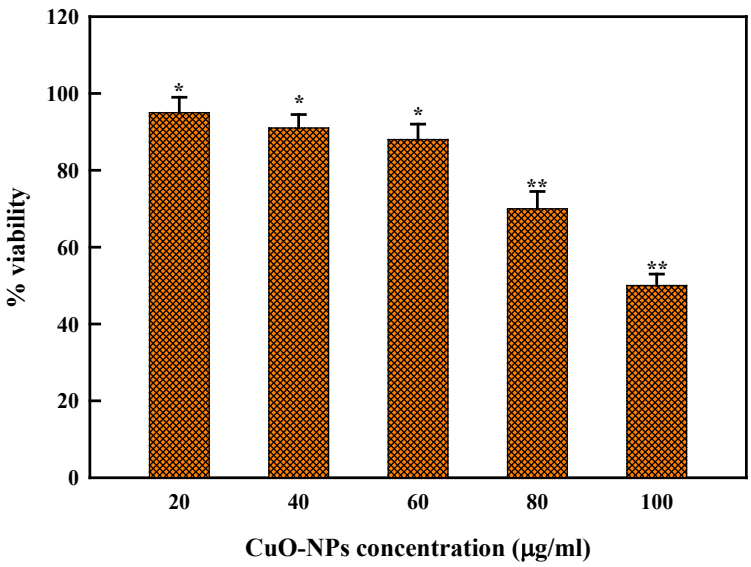

Fig. 11 Cytotoxicity of CuO-NPs against brine shrimp

The primary organic contaminants in wastewater, azo dyes are thought to be extremely hazardous, mutagenic, carcinogenic, teratogenic [95, 141-143]. In this study, dyes RR195 and RY145 were used as a model azo dye compounds to examine the catalytic effectiveness of SH assisted CuO-NPs as a nanocatalyst in the presence of $NaBH_4$ well elucidated by time-dependent absorption curves (Fig.12). Firstly, the absorption peaks of dyes RR195 and RY145 were documented at 530 nm and 430 nm, respectively. The degradation experiment was conducted after recording their intensities as a function of time. The addition of CuO-NPs alone noted a small decrease in the intensities of dyes RR195 and RY145 (data not shown). Also, there was only a 7.94% and 13.22% fall in RR195 and RY145 by 50 minutes under $NaBH_4$ alone in the breakdown of azo dyes, indicating an incomplete dye breakdown (Fig.12: a1–a2) attributable to simple surface absorption (Reaction 1), instead of dye breakdown. However, when $NaBH_4$ coupled CuO-NPs were added to the dye solution, there was a significant drop in the intensity of the absorption (Fig.12: b1–b2). As the reaction proceeded, the dye hue disappeared turning the reaction mixture to clear solution, indicating the breakdown of dyes. The rate of degradation of dyes RR195 and RY145 were found to be 93% and 91%, respectively. However, the appearance of lower band peak following the reduction process shows that the azo dye decolorization was achieved by the breakdown of azo structure as opposed to merely physical adsorption, indicating the conversion of azo dyes into the equivalent amine compounds (Reaction 2). Since the dye concentration at a given time (C_t) was directly proportional to the absorbance values at that time (A_t), the reaction followed pseudo-first-order kinetics. From the linearity of $\ln(A_t/A_0)$ vs t plot, the kinetic rate constants (k) of RR195 and

RY145 was found to be as 0.0941 and 0.0220 min^{-1}, respectively calculated straight for the straight-line slope (Fig.12: c1–c2). It is important to note that dye RR195 degraded relatively faster than dye RY145 which may possibly be due to the steric barrier of additional groups close to -N=N- in the latter molecule. The three steps can be used to describe the reduction mechanism: (i) Adsorption of azo elements and BH_4^- by CuO-NPs, (ii) the transfer of electron (e^-) from BH_4^- to dye molecules via CuO-NPs, (iii) the reaction of Cu^{2+} with dye molecules and (iv) the conversion of colorful dye (–N=N–) into monochrome amines (–NH_2 + H_2N–) compounds. Similar mechanism of dye degradation was also reported by [16, 17, 144].

$$R_1\text{-}N{=}N\text{-}R_2 \rightarrow R_1\text{-}HN{=}NH\text{-}R_2 \text{ (Reaction 1)}$$

$$R_1\text{–}N{=}N\text{–}R_2 \rightarrow R_1\text{–}NH_2 + H_2N\text{–}R_2 \text{ (Reaction 2)}$$

As a result, Scheme 1 updates the reaction mechanism with precise specifications. Here, SH serves as a stabilizer to prevent any aggregation and maintain the catalytic activity of the biosynthesized nanoparticle. The dye elements are adsorbed on the exterior of CuO-NPs due to the presence of biopolymer clad nanoparticles, without affecting their function [145]. Additionally, as the reducing agents such as $NaBH_4$ were introduced into the reaction system, the nanoparticles instantly absorbed them, reducing the reductive strength significantly. However, the capping of SH on the nanoparticle validated the regular electron flow from nucleophilic $NaBH_4$ to dye oxidation [145]. As a result, the azo dyes were easily absorbed by electrons, causing a redox reaction that destroyed dye chromophore structure and led to the production of amine species [146]. Schematically, Scheme 2 illustrates the advantage of biopolymer with respect to dye degradation using SH-assisted CuO-NPs via electron transfer from $NaBH_4$ nucleophile.

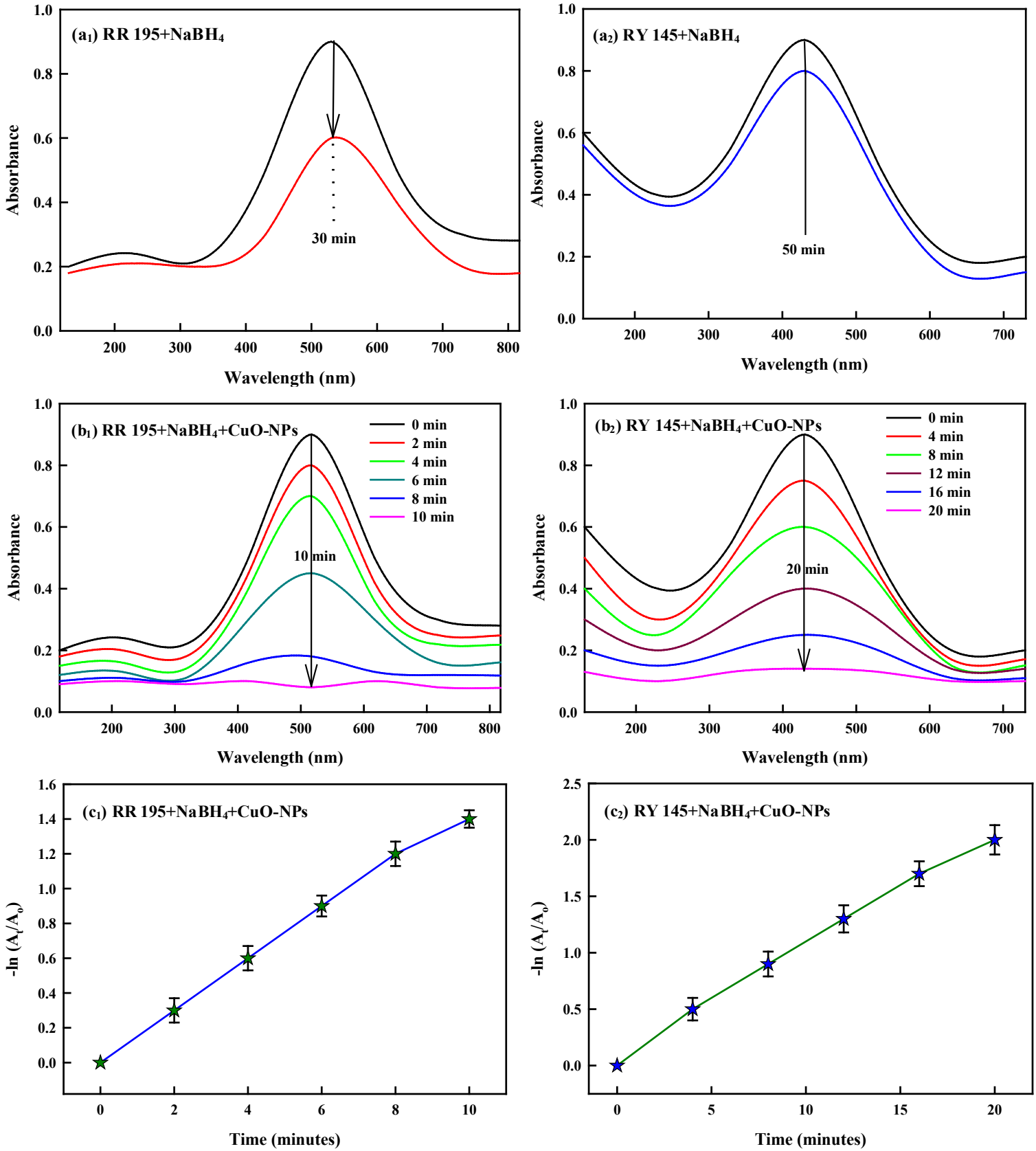

Fig. 12 Absorption with (a_2–b_2) and without (a_1–b_1) CuO-NPs, and linear relationship of $\ln(A_t/A_o)$ (c_1–c_2) for the catalytic dye reduction.

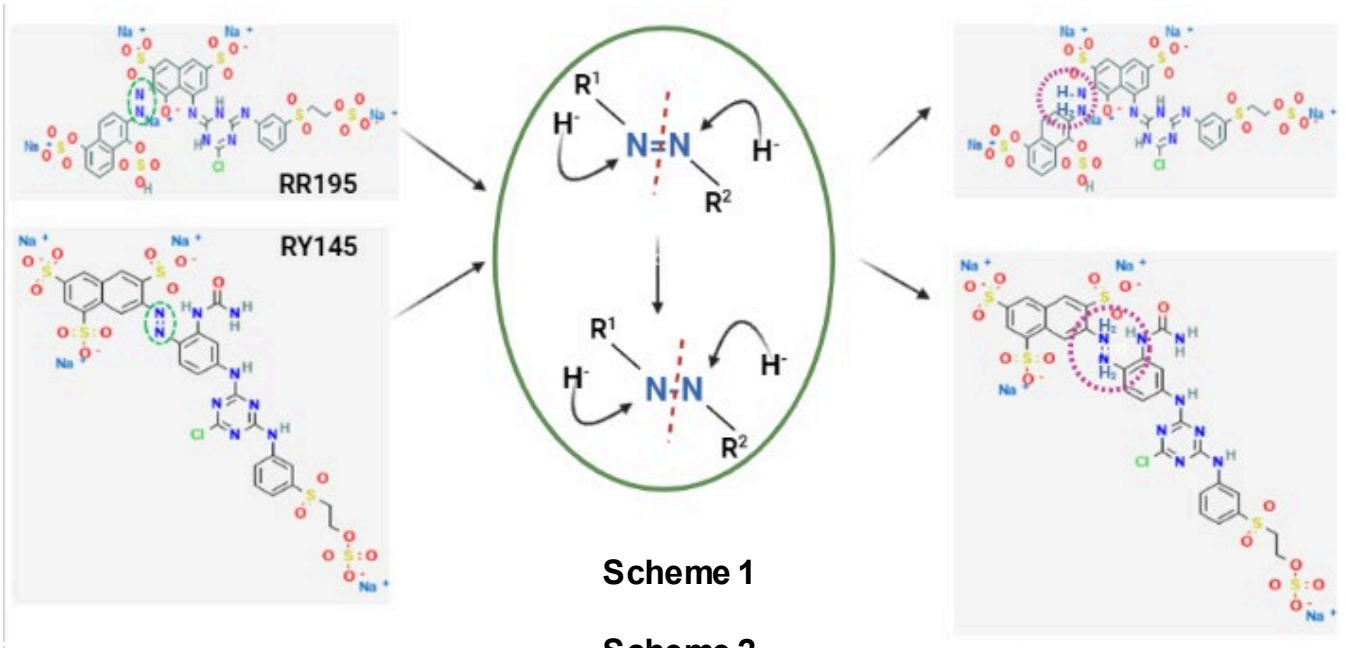

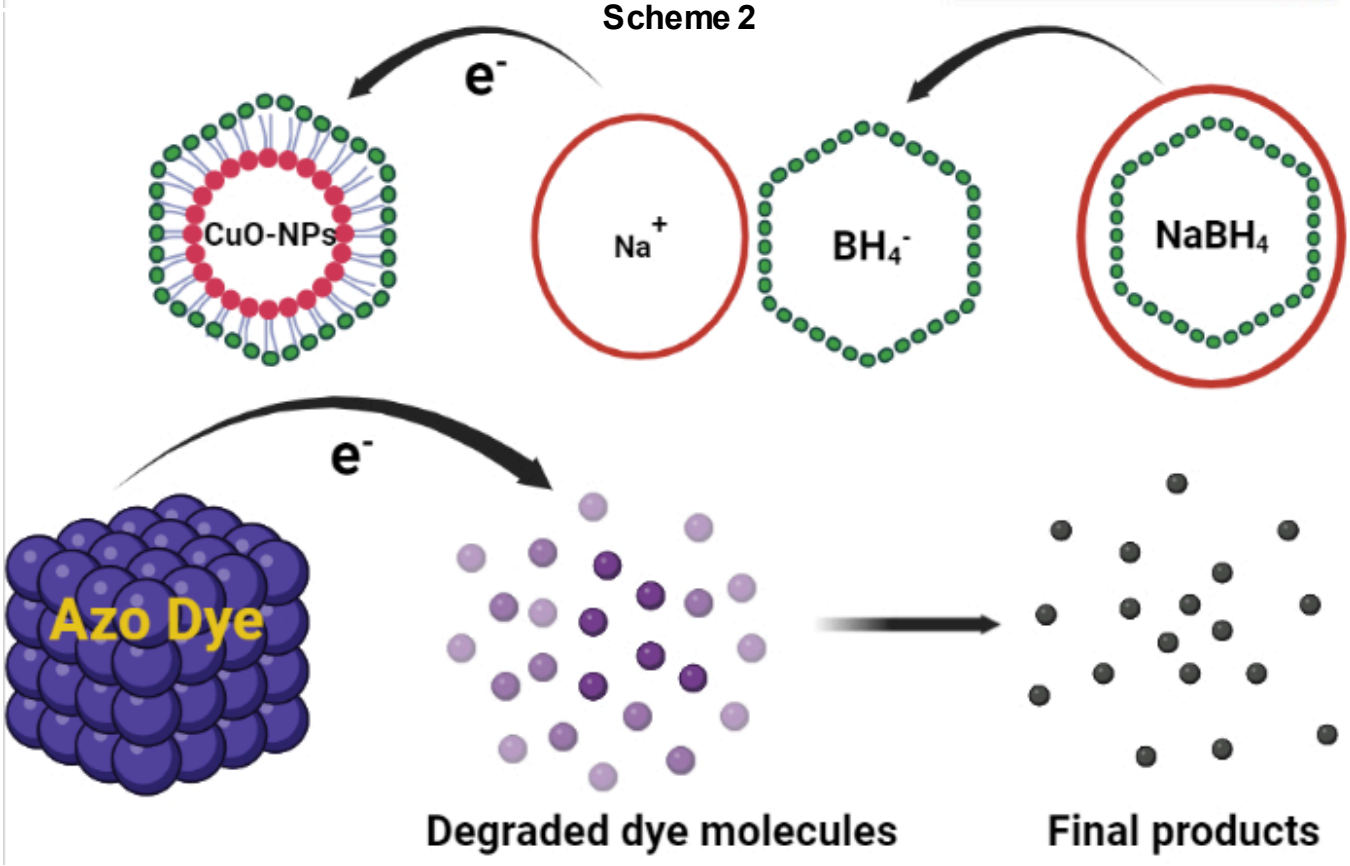

Scheme 1 Using a biocatalyst with a $NaBH_4$ coupling, RR195 and RY145 are effectively degraded.

Scheme 2 provides an illustration of the process involved in the use of CuO-NPs by $NaBH_4$ nucleophile to move electrons in favour of biopolymer in dye decomposition.

4. Conclusion

In conclusion, SH-assisted CuO-NPs were formed, for the first time, in an environmentally friendly, one-pot method in which SH macromolecules served as stabilizing and reducing agents for CuO-NPs in the SH-matrix. Without employing any harmful reagents, the reaction parameters were standardized to maximize the yield of CuO-NPs. The CuO-NPs fabricated using the sustainable chemistry approach were extremely crystalline, well-capped and well-dispersed CuO-NPs by SH-macromolecules and have a spherical/oval shape measuring 17.4±1.3 nm with an elemental composition of 29.49%. The FT-IR spectra exhibited the presence of many carboxyl and hydroxyl groups which helped in the maintenance of monodispersed state by electrostatic repulsion. The biosynthesized CuO-NPs exhibited notable bactericidal (*E. coli* {inhibition zone 27mm; biofilm inhibition 85.32%; *S. aureus* [inhibition zone 22mm; biofilm inhibition 71.2%}) and antioxidant [FRSA (70±2.3%), TAC (85±0.26%), TRP (76±0.35%), ABTS (400μm TEAC), FRAP (423 μm TEAC)] activities. The increased activities of enzymes like urease (68±2.1%), lipase (70±2.3%), peroxidase (0.59 mM/min/mg), ROS/RNS 3400 counts of relative probe fluorescence, metal chelation (33%) and cell leakage assays of protein (*E. coli* 112 μg/ml; *S. aureus* 78 μg/ml) and nucleic acids (*E. coli* OD 0.2; *S. aureus* OD 0.11) were reported in the presence of CuO-NPs. Furthermore, the CuO-NPs exhibited enhanced anti-diabetic activity against enzymes α-amylase (72±1.2%) and α-glucosidase (70±2.1%). Also, the combination of intrinsic time-dependent absorptive spectra and mechanics of pseudo-first-order reaction kinetics demonstrated biosynthesized CuO-NPs as efficient nanocatalyts for azo dyes decomposition (91-93% rate of degradation) and hold great promise in the fields of industrial wastewater treatment.

Author contributions

Conceptualization, T.C.; formal analysis, T.C.; investigation, T.C.; methodology, T.C., data curation, T.C., C.R.; validation, T.C., W.J.; writing—original draft, T.C.; writing—review and editing, I.N; writing—review and editing, T.C., C.R., R.K.V.R, J.J., W.J., C.K. All authors have read and agreed to the published version of the manuscript.

Acknowledgments

The first author is sincerely grateful to Mar Athanasios College for Advanced Studies Tiruvalla (MACFAST) for offering facilities for laboratories and infrastructural support.

Conflicts of Interest

The authors declare no conflict of interest.

References

[1] T. Cherian, D. Maity, R.T. Rajendra Kumar, G. Balasubramani, C. Ragavendran, S. Yalla, R. Mohanraju, W.J.G.M. Peijnenburg, Green chemistry based gold nanoparticles synthesis using the marine bacterium *Lysinibacillus odysseyi* PBCW2 and their multitudinous activities, Nanomat. 12 (2022) 2940.

[2] T. Cherian, K. Ali, S. Fatima, Q. Saquib, S.M. Ansari, H.A. Alwathnani, A.A. Al-Khedhairy, M. Al-Shaeri, J. Musarrat, *Myristica fragrans* bio-active ester functionalized ZnO nanoparticles exhibit antibacterial and antibiofilm activities in clinical isolates, J. Microbiol. Methods. 166 (2019) 105716.

[3] T. Cherian, K. Ali, Q. Saquib, M. Faisal, R. Wahab, J. Musarrat, *Cymbopogon citratus* functionalized green synthesis of CuO nanoparticles: Novel prospects as antibacterial and antibiofilm agents, Biomol. 10 (2020) 169.

[4] A. Verma, S.P. Gautam, K.K. Bansal, N. Prabhakar and J.M. Rosenholm, Green Nanotechnology: Advancement in phytoformulation research, Medicines 6 (1) (2019) 39; https://doi.org/10.3390/medicines6010039.

[5] S. Ghotekar, S. Pansambal, M. Bilal, S.S. Pingale, R. Oza, Environmentally friendly synthesis of Cr_2O_3 nanoparticles: Characterization, applications and future perspective- a review, Case Studies in Chemical and Environmental Engineering 3 (2021) 100089.

[6] T. Pagar, S. Ghotekar, S. Pansambal, R. Oza, B.P. Marasini, Facile plant extract mediated eco-benevolent synthesis and recent applications of CaO-NPs: a state-of the- art review, J. Chem. Rev. 2 (3) (2020) 201–210, https://doi.org/10.22034/JCR.2020.107355.

[7] X. Zhang, C. Huang, S. Mahmud, X. Guo, X. Hu, Y. Jing, S. Su, J. Zhu, Sodium alginate fasten cellulose nanocrystal Ag@AgCl ternary nanocomposites for the synthesis of antibacterial hydrogels, Compos. Commun. 25 (2021) 100717.

[8] A. Naghizadeh, Z.M. Mizwari, S.M. Ghoreishi, S. Lashgari, S. Mortazavi-Derazkola, B. Rezaie, Biogenic and eco-benign synthesis of silver nanoparticles using jujube core extract and its performance in catalytic and pharmaceutical applications: Removal of industrial contaminants and in-vitro antibacterial and anticancer activities, Environ. Technol. Innov. 23 (2021) 101560.

[9] M. Shirzadi-Ahodashti, Z.M. Mizwari, Z. Hashemi, S. Rajabalipour, S.M. Ghoreishi, S. Mortazavi-Derazkola, M.A. Ebrahimzadeh, Discovery of high antibacterial and catalytic activities of biosynthesized silver nanoparticles using *C. fruticosus* (CF-AgNPs) against multi-drug resistant clinical strains and hazardous pollutants, Environ. Technol. Innov. 23 (2021) 101607.

[10] S.A. Akintelu, S.C. Olugbeko, A.S. Folorunso, A review on synthesis, optimization, characterization and antibacterial application of gold nanoparticles synthesized from plants, Int. Nano Lett. (2020) 1–12.

[11] F. Abdelghaffar, Biosorption of anionic dye using nanocomposite derived from chitosan and silver nanoparticles synthesized via cellulosic banana peel bio-waste, Environ. Technol. Innov. 24 (2021) 101852.

[12] K.C. Majhi, M. Yadav, Chapter 5 - synthesis of inorganic nanomaterials using carbohydrates. In: Inamuddin Boddula, R., Ahamed, M.I., Asiri, A.M. (Eds.), Green Sustainable Process for Chemical and Environmental Engineering and Science. Elsevier (2021) pp. 109–135.

[13] K.M.F. Hasan, H. Wang, S. Mahmud, C. Genyang, Coloration of aramid fabric via in-situ biosynthesis of silver nanoparticles with enhanced antibacterial effect, Inorg. Chem. Commun. 119 (2020a) 108115.

[14] K.M.F. Hasan, H. Wang, S. Mahmud, M.A. Jahid, M. Islam, W. Jin, C. Genyang, Colorful and antibacterial nylon fabric via in-situ biosynthesis of chitosan mediated nanosilver, J. Mater. Res. Technol. 9 (6) (2020b) 16135–16145.

[15] Y. Xiong, L. Huang, S. Mahmud, F. Yang, H. Liu, Bio-synthesized palladium nanoparticles using alginate for catalytic degradation of azo-dyes, Chin. J. Chem. Eng. 28 (5) (2020) 1334–1343.

[16] H. Wan, C. Li, S. Mahmud, H. Liu, Kappa carrageenan reduced-stabilized colloidal silver nanoparticles for the degradation of toxic azo compounds, Colloids Surf. A 616 (2021a) 126325.
[17] H. Wan, Z. Liu, Q. He, D. Wei, S. Mahmud, H. Liu, Bioreduction (AuIII to Au0) and stabilization of gold nanocatalyst using Kappa carrageenan for degradation of azo dyes, Int. J. Biol. Macromol. 176 (2021b) 282–290.
[18] S. Mahmud, N. Pervez, M.A. Taher, K. Mohiuddin, H.-H. Liu, Multifunctional organic cotton fabric based on silver nanoparticles green synthesized from sodium alginate, Textile Res. J. 90 (11–12) (2020) 1224–1236.
[19] J. Chen, Y. Liu, Y. Xiong, D. Wei, J. Peng, S. Mahmud, H. Liu, Konjac glucomannan reduced-stabilized silver nanoparticles for mono-azo and di-azo contained wastewater treatment, Inorg. Chim. Acta 515 (2021a) 120058.
[20] J. Chen, D. Wei, L. Liu, J. Nai, Y. Liu, Y. Xiong, J. Peng, S. Mahmud, H. Liu, Green synthesis of konjac glucomannan templated palladium nanoparticles for catalytic reduction of azo compounds and hexavalent chromium, Mater. Chem. Phys. 267 (2021b) 124651.
[21] Y. Xiong, H. Wan, M. Islam, W. Wang, L. Xie, S. Lü, S.M. Fijul Kabir, H. Liu, S. Mahmud, Hyaluronate macromolecules assist bioreduction (Au^{III} to Au^{0}) and stabilization of catalytically active gold nanoparticles for azo contaminated wastewater treatment, Environ. Technol. Innov. 24 (2021) 102053.
[22] J. Sequeira, B.S. Rao, P.R. Kedia, Efficacy of sodium hyaluronate for temporomandibular joint disorder by single-puncture arthrocentesis, J. Maxillofacial Oral Surg. 18 (1) (2019) 88.
[23] M.H. El-Dakdouki, D.C. Zhu, K. El-Boubbou, M. Kamat, J. Chen, W. Li, X. Huang, Development of multifunctional hyaluronan-coated nanoparticles for imaging and drug delivery to cancer cells, Biomacromol. 13 (4) (2012) 1144–1151.
[24] F. Namvar, S. Azizi, H.S. Rahman, R. Mohamad, A. Rasedee, M. Soltani, R.A. Rahim, Green synthesis, characterization, and anticancer activity of hyaluronan/zinc oxide nanocomposite, OncoTargets Therapy. 9 (2016) 4549.
[25] K.M. Rao, M. Suneetha, S. Zo, K.H. Duck, S.S. Han, One-pot synthesis of ZnO nanobelt-like structures in hyaluronan hydrogels for wound dressing applications, Carbohydr. Polymers. 223 (2019) 115124.
[26] G. Khachatryan, K. Khachatryan, J. Grzyb, M. Fiedorowicz, Formation and properties of hyaluronan/nano Ag and hyaluronan-lecithin/nano Ag films, Carbohydr. Polymers. 151 (2016) 452–457.
[27] N. Xia, Y. Cai, T. Jiang, J. Yao, Green synthesis of silver nanoparticles by chemical reduction with hyaluronan, Carbohydr. Polymers. 86 (2) (2011) 956–961.

[28] R. Abdel-Mohsen, L. Hrdina, G. Burgert, R.M. Krylová, A. Abdel-Rahman, M. Krejčová, L. Beneš Steinhart, Green synthesis of hyaluronan fibers with silver nanoparticles, Carbohydr. Polymers 89 (2) (2012) 411–422.
[29] J.-P. Deng, S.-H. Li, S.-T. Chang, Y.-C. Shih, Hyaluronan-assisted synthesis of silver nanoparticles and nanowires, Res. Chem. Intermed. 45 (1) (2019) 119–125.
[30] X. Zhang, M. Yao, M. Chen, L. Li, C. Dong, Y. Hou, H. Zhao, B. Jia, F. Wang, Hyaluronic acid-coated silver nanoparticles as a nanoplatform for in vivo imaging applications, ACS Appl. Mater. Interfaces. 8 (39) (2016) 25650–25653.
[31] H.-J. Li, A.-Q. Zhang, L. Sui, D.-J. Qian, M. Chen, Hyaluronan/tween 80-assisted synthesis of silver nanoparticles for biological application, J. Nanoparticle Res. 17 (2) (2015) 1–13.
[32] N.Q. Hien, D. Van Phu, N.N. Duy, Radiation synthesis and characterization of hyaluronan capped gold nanoparticles, Carbohydr. Polymers. 89 (2) (2012) 537–541.
[33] H.S. Han, K.Y. Choi, H. Lee, M. Lee, J.Y. An, S. Shin, S. Kwon, D.S. Lee, J.H. Park, Gold-nanoclustered hyaluronan nano-assemblies for photothermally maneuvered photodynamic tumor ablation, ACS Nano. 10 (12) (2016) 10858–10868.
[34] M.M. Kemp, A. Kumar, S. Mousa, T.-J. Park, P. Ajayan, N. Kubotera, S.A. Mousa, R.J. Linhardt, Synthesis of gold and silver nanoparticles stabilized with glycosaminoglycans having distinctive biological activities, Biomacromolecul. 10 (3) (2009) 589–595.
[35] N. Verma and N. Kumar, Synthesis and biomedical applications of copper oxide nanoparticles: an expanding horizon, ACS Biomater. Sci. Eng. 5 (2019) 1170–1188.
[36] W. M. Rangel, R.A.A.B. Santa and H.G. Riella, A facile method for synthesis of nanostructured copper(II) oxide by co-precipitation, J. Mater. Res. Technol. 9 (2020) 994–1004.
[37] K. Velsankar, S. Suganya, P. Muthumari, S. Mohandoss and S. Sudhahar, Ecofriendly green synthesis, characterization and biomedical applications of CuO nanoparticles synthesized using leaf extract of *Capsicum frutescens*, J. Environ. Chem. Eng. 9 (2021) 106299.
[38] A. Waris, M. Din, A. Ali, M. Ali, S. Afridi, A. Baset and A. U. Khan, A comprehensive review of green synthesis of copper oxide nanoparticles and their diverse biomedical applications, Inorg. Chem. Commun. 123 (2021) 1387–7003.

[39] D. Rehana, D. Mahendiran, R. S. Kumar and A. K. Rahiman, Evaluation of antioxidant and anticancer activity of copper oxide nanoparticles synthesized using medicinally important plant extracts, Biomed. Pharmacother. 89 (2017) 1067–1077.

[40] S.S. Salem and A. Fouda, Green synthesis of metallic nanoparticles and their prospective biotechnological applications: an overview, Biol. Trace Elem. Res. 199 (2021) 344–370.

[41] M. Naseer, U. Aslam, B. Khalid and B. Chen, Green route to synthesize Zinc Oxide Nanoparticles using leaf extracts of *Cassia fistula* and *Melia azadarach* and their antibacterial potential, Sci. Rep. 10 (2020) 1–10.

[42] C. Dipankar and S. Murugan, The green synthesis, characterization and evaluation of the biological activities of silver nanoparticles synthesized from *Iresine herbstii* leaf aqueous extracts, Colloids Surf., B. 98 (2012) 112–119.

[43] R. Javed, M. Ahmed, I. ul Haq, S. Nisa and M. Zia, PVP and PEG doped CuO nanoparticles are more biologically active: Antibacterial, antioxidant, antidiabetic and cytotoxic perspective, Mater. Sci. Eng., C. 79 (2017) 108–115.

[44] M.N. Karim, M. Singh, P. Weerathunge, P. Bian, R. Zheng, C. Dekiwadia, T. Ahmed, S. Walia, E. Della Gaspera and S. Singh, Visible-light-triggered reactive-oxygen-species mediated antibacterial activity of peroxidase-mimic CuO nanorods, ACS Appl. Nano Mater. 1 (2018) 1694–1704.

[45] S. Kabir, R. Cueto, S. Balamurugan, L.D. Romeo, J.T. Kuttruff, B.D. Marx, I.I. Negulescu, Removal of acid dyes from textile wastewaters using fish scales by absorption process, Clean Technol. 1 (1) (2019) 311–324.

[46] T.U. Rashid, S.F. Kabir, M.C. Biswas, M.R. Bhuiyan, Sustainable wastewater treatment via dye–surfactant interaction: a critical review, Ind. Eng. Chem. Res. 59 (21) (2020) 9719–9745.

[47] F. Qu, A. Cao, Y. Yang, S. Mahmud, P. Su, J. Yang, Z. He, Q. Lai, L. Zhu, Z. Tu, Q. Wang, Z. Xiong, S. Zhao, Hierarchically superhydrophilic poly(vinylidene fluoride) membrane with self-cleaning fabricated by surface mineralization for stable separation of oily wastewater, J. Membr. Sci. 640 (2021) 119864.

[48] F. Ghanbari, M. Moradi, Electrooxidation Processes for Dye Degradation and Colored Wastewater Treatment. CRC Press LLC, London (2016).

[49] J. Dotto, M.R. Fagundes-Klen, M.T. Veit, S.M. Palacio, R. Bergamasco, Performance of different coagulants in the coagulation/flocculation process of textile wastewater, J. Cleaner Prod. 208 (2019) 656–665.

[50] P.S. Kumar, A. Saravanan, Sustainable Wastewater Treatments in Textile Sector, Sustainable Fibres and Textiles. Elsevier (2017) pp. 323–346.
[51] Y. Tian, Y. Shu, X. Zhang, S. Mahmud, J. Zhu, S. Su, Electrospun PVDF-Ag@ AgCl porous fiber membrane: stable antifoul and antibacterial surface, Surface Innov. 9 (2–3) (2020) 156–165.
[52] X. Guo, S. Mahmud, X. Zhang, N. Yu, K.F. Hasan, One-pot green synthesis of Ag@ AgCl nanoparticles with excellent photocatalytic performance, Surface Innov. 9 (5) (2021) 277–284.
[53] A. Akbari, M. Amini, A. Tarassoli, B. Eftekhari-Sis, N. Ghasemian, E. Jabbari, Transition metal oxide nanoparticles as efficient catalysts in oxidation reactions, Nano-Struct. Nano-Objects 14 (2018) 19–48.
[54] M. Nasrollahzadeh, M. Sajjadi, S. Iravani, R.S. Varma, Carbon-based sustainable nanomaterials for water treatment: State-of-art and future perspectives, Chemosp. 263 (2021a) 128005.
[55] M. Nasrollahzadeh, M. Sajjadi, S. Iravani, R.S. Varma, Green-synthesized nanocatalysts and nanomaterials for water treatment: Current challenges and future perspectives, J. Hard Mater. 401 (2021b) 123401.
[56] M. Sorbiun, E. S. Mehr, A. Ramazani and S. T. Fardood, Green synthesis of zinc oxide and copper oxide nanoparticles using aqueous extract of oak fruit hull (jaft) and comparing their photocatalytic degradation of basic violet 3, Int. J. Environ. Res. 12 (2018) 29–37.
[57] E.S. Mehr, M. Sorbiun, A. Ramazani and S. T. Fardood, Plant-mediated synthesis of zinc oxide and copper oxide nanoparticles by using *Ferula goangulata* (schlecht) boiss extract and comparison of their photocatalytic degradation of Rhodamine B (RhB) under visible light irradiation, J. Mater. Sci.: Mater. Electron. 29 (2018) 1333–1340.
[58] A. Muthuvel, M. Jothibas and C. Manoharan, Synthesis of copper oxide nanoparticles by chemical and biogenic methods: photocatalytic degradation and in vitro antioxidant activity, Nanotechnol. Environ. Eng. 5 (2020) 1–19.
[59] G. Bibi, N. Ullah, A. Mannan and B. Mirza, Antitumor, cytotoxic and antioxidant potential of *Aster thomsonii* extracts, Afr. J. Pharm. Pharmacol. 5 (2011) 252–258.
[60] M.A. Sheliya, R. Begum, K.K. Pillai, V. Aeri, S.R. Mir, A. Ali, M. Sharma, In vitro α-glucosidase and α-amylase inhibition by aqueous, hydroalcoholic, and alcoholic extract of *Euphorbia hirta* L., Drug Dev. Ther. 7 (2016) 26.

[61] B. Saleem, M. Islam, H. Saeed, F. Imtiaz, M. Asghar, Z. Saleem, A. Mehmood,S. Naheed, Investigations of *Acacia modesta* Wall. leaves for *in vitro* antidiabetic, proliferative and cytotoxic effects, Braz. J. Pharm. Sci. 54 (2018) 2.

[62] M. Biglar, K. Soltani, F. Nabati, R. Bazl, F. Mojab and M. Amanlou, A preliminary investigation of the jack-bean urease inhibition by randomly selected traditionally used herbal medicine, Iran. J. Pharm. Res. 11 (2012) 831.

[63] G. J. McDougall, N. N. Kulkarni and D. Stewart, Berry polyphenols inhibit pancreatic lipase activity in vitro, Food Chem. 115 (2009) 193–199.

[64] H. Fatima, K. Khan, M. Zia, T. Ur-Rehman, B. Mirza and I.-u. Haq, Extraction optimization of medicinally important metabolites from *Datura innoxia* Mill.: an in vitro biological and phytochemical investigation, BMC Complementary Altern. Med. 15 (2015) 1–18.

[65] H. Zafar, A. Ali, J. S. Ali, I. U. Haq and M. Zia, Effect of ZnO nanoparticles on *Brassica nigra* seedlings and stem explants: growth dynamics and antioxidative response, Front. Plant Sci. 7 (2016) 535.

[66] M. Shah, M.A. Ullah, S. Drouet, M. Younas, D. Tungmunnithum, N. Giglioli-Guivarćh, C. Hano and B.H. Abbasi, Interactive effects of light and melatonin on biosynthesis of silymarin and anti-inflammatory potential in callus cultures of *Silybum marianum* (L.) Gaertn, Molecules 24 (2019) 1207.

[67] M. Nazir, D. Tungmunnithum, S. Bose, S. Drouet, L. Garros, N. Giglioli-Guivarćh, B. H. Abbasi and C. Hano, Differential production of phenylpropanoid metabolites in callus cultures of *Ocimum basilicum* L. with distinct in vitro antioxidant activities and in vivo protective effects against UV stress, J. Agric. Food Chem. 67 (2019) 1847–1859.

[68] B. Shanmuganathan, K. Pandima Devi, Evaluation of the nutritional profile and antioxidant and anti-cholinesterase activities of *Padina gymnospora* (Phaeophyceae), Eur J Phycol. 51 (2016) 482–490. https ://doi.org/10.1080/09670 262.2016.1218938.

[69] R.J. Ruch, S.J. Cheng, J.E. Klaunig, Prevention of cytotoxicity and inhibition of intercellular communication by antioxidant catechins isolated from Chinese green tea, Carcinogen 10 (1989) 1003-1008.

[70] L. Lagrimini, Plant peroxidases: under-and over-expression in transgenic plants and physiological consequences, Plant Peroxidases 1980 (1990) 59–69.

[71] V. De Matteis, M. Cascione, C.C. Toma, S. Leporatti, Silver nanoparticles: synthetic routes, in vitro toxicity and theranostic applications for cancer disease, Nanomaterials (Basel) 8 (2018) 319. doi:10.3390/nano8050319.

[72] C.N. Baker, S.A. Stocker, D.H. Culver, C. Thornsberry, Comparison of the E Test to agar dilution, broth microdilution, and agar diffusion susceptibility testing techniques by using a special challenge set of bacteria, J. Clin. Microbiol. 29 (1991) 533–538.

[73] J. Hausdorfer, E. Sompek, F. Allerberger, M. Dierich, S. Rüsch-Gerdes, E-test for susceptibility testing of *Mycobacterium tuberculosis*, Int. J. Tuberc. Lung Dis. 2 (1998) 751–755.

[74] S. Magaldi, S. Mata-Essayag, C.H. de Capriles, C. Pérez, M. Colella, C. Olaizola, Y. Ontiveros, Well diffusion for antifungal susceptibility testing, Int. J. Infect. Dis. 8 (2004) 39–45.

[75] C. Valgas, S.M.d. Souza, E.F. Smânia, A. Jr. Smânia, Screening methods to determine antibacterial activity of natural products, Braz. J. Microbiol. 38 (2007) 369–380.

[76] F. Duman, I. Ocsoy, F.O. Kup, Chamomile flower extract-directed CuO nanoparticle formation for its antioxidant and DNA cleavage properties, Mater. Sci. Eng. C 60 (2016) 333–338.

[77] S.-H. Kim, H.-S. Lee, D.-S. Ryu, S.-J. Choi, D.-S. Lee, Antibacterial activity of silver-nanoparticles against *Staphylococcus aureus* and *Escherichia coli*, Microbiol. Biotechnol. Lett. 39 (2011) 77–85.

[78] A. Álvarez-Ordóñez, A. Carvajal, H. Arguello, F. Martínez-Lobo, G. Naharro, P. Rubio, Antibacterial activity and mode of action of a commercial citrus fruit extract, J. Appl. Microbiol. 115 (2013) 50–60.

[79] S. Lee, K. Na, Oleic acid conjugated polymeric photosensitizer for metastatic cancer targeting in photodynamic therapy, Biomater. Res. 24 (2020) 1–8.

[80] X. Deng, M. Cao, J. Zhang, K. Hu, Z. Yin, Z. Zhou, X. Xiao, Y. Yang, W. Sheng, Y. Wu, *et al.*, Hyaluronic acid-chitosan nanoparticles for co-delivery of MiR-34a and doxorubicin in therapy against triple negative breast cancer, Biomaterials 35 (2014) 4333–4344.

[81] S. Blanco, S. Peralta, M.E. Morales, E. Martínez-Lara, J.R. Pedrajas, H. Castán, M.Á. Peinado, M.A. Ruiz, Hyaluronate nanoparticles as a delivery system to carry neuroglobin to the brain after stroke, Pharmaceutics 12 (1) (2020) 40.

[82] C. Saraiva, C. Praca, R. Ferreira, T. Santos, L. Ferreira, L. Bernardino, Nanoparticle-mediated brain drug delivery: Overcoming blood-brain barrier to treat neurodegenerative diseases, J. Control. Release. 235 (2016) 34–47.

[83] K. Ganesan, V.K. Jothi, A. Natarajan, A. Rajaram, S. Ravichandran, S. Ramalingam, Green synthesis of Copper oxide nanoparticles decorated with graphene oxide for anticancer activity and catalytic applications, Arabian J. Chem. 13 (2020) 6802–6814.

[84] N.M. Zain, A.G.F. Stapley, G. Shama, Green synthesis of silver and copper nanoparticles using ascorbic acid and chitosan for antimicrobial applications, Carbohydr. Polym. 112 (2014) 195–202, doi:10.1016/j.carbpol.2014.05.081.

[85] S. Chaudhary, D. Rohilla, A. Umar, N. Kaur, A. Shanavas, Synthesis and characterizations of luminescent copper oxide nanoparticles: toxicological profiling and sensing applications, Ceram. Int. 45 (2019) 15025–15035.

[86] A. Shafiqa, A.A. Aziz, B. Mehrdel, Nanoparticle optical properties: Size dependence of a single gold spherical nanoparticle, Journal of Physics: Conference Series. IOP Publishing (2018) 012040.

[87] S.K. Das, B.K. Chandra, R.A. Molla, M. Sengupta, S.M. Islam, A. Majee, A. Bhaumik, CuO grafted triazine functionalized covalent organic framework as an efficient catalyst for CC homo coupling reaction, Mol. Catal. 480 (2020) 110650.

[88] M. Guo, W. Li, F. Yang, H. Liu, Controllable biosynthesis of gold nanoparticles from a *Eucommia ulmoides* bark aqueous extract, Spectrochim. Acta Part A: Mol. Biomol. Spectr. 142 (2015) 73–79.

[89] K. Kartini, A. Alviani, D. Anjarwati, A.F. Fanany, J. Sukweenadhi, and C. Avanti, Process optimization for green synthesis of silver nanoparticles using Indonesian medicinal plant extracts, Processes 8 (8) (2020) 998. doi:10.3390/pr8080998.

[90] P.K. Dikshit, J. Kumar, A.K. Das, S. Sadhu, S. Sharma, S. Singh, P.K. Gupta and B.S. Kim, Green synthesis of metallic nanoparticles: Applications and Limitations, Catalysts 11 (8) (2021) 902; https://doi.org/10.3390/catal11080902.

[91] M.M. Said, M. Rehan, S.M. El-Sheikh, M.K. Zahran, M.S. Abdel-Aziz, M. Bechelany, A. Barhoum, Multifunctional hydroxyapatite/silver nanoparticles/cotton gauze for antimicrobial and biomedical applications, Nanomaterials 11 (2021) 429.

[92] Q. Song, Y. Wang, L. Huang, M. Shen, Y. Yu, Q. Yu, Y. Chen, J. Xie, Review of the relationships among polysaccharides, gut microbiota, and human health, Food Res. Int. 140 (2021) 109858.

[93] M. Fernandes, A.P. Souto, F. Dourado, M. Gama, Application of bacterial cellulose in the Textile and Shoe Industry: Development of biocomposites, Polysaccharides 2 (2021) 34.

[94] R. Mongkholrattanasit, C. Klaichoi, N. Rungruangkitkrai, Printing silk fabric with acid dye using a new thickening agent, J. Nat. Fibers (2021) in press.
[95] H. Chen, Y. Jia, Q. Guo, Polysaccharides and polysaccharide complexes as potential sources of antidiabetic compounds: A review. In Bioactive Natural Products; Atta-ur-Rahman, Ed.; Studies in Natural Products Chemistry; Elsevier: Amsterdam, The Netherlands (2020) 199–220.
[96] C. Wang, X. Gao, Z. Chen, Y. Chen, H. Chen, Preparation, characterization and application of polysaccharide-based metallic nanoparticles: A review, Polymers 9 (2017) 689.
[97] M. Fernandes, J. Padrão, A.I. Ribeiro, R.D.V. Fernandes, L. Melro, T. Nicolau, B. Mehravani, C. Alves, R. Rodrigues and A. Zille, Polysaccharides and metal nanoparticles for functional textiles: A review, Nanomaterials 12 (6) (2022) 1006; https://doi.org/10.3390/nano12061006.
[98] D.O.B. Apriandanu and Y. Yulizar, *Tinospora crispa* leaves extract for the simple preparation method of CuO nanoparticles and its characterization, Nano-Struct. Nano- Objects, 20 (2019) 100401.
[99] Y. Yulizar, I. Latifah, R. Bakri and D. Apriandanu, Plants extract mediated synthesis of copper (II) oxide nanoparticles using *Oldenlandia corymbosa* L. leaf, AIP Conf. Proc. 2023 (2018) 020097.
[100] J. Iqbal, A. Andleeb, H. Ashraf, B. Meer, A. Mehmood, H. Jan, G. Zaman, M. Nadeem, S. Drouet, H. Fazal, N.G.-Guivarćh, C. Hano and B.H. Abbasi, Potential antimicrobial, antidiabetic, catalytic, antioxidant and ROS/RNS inhibitory activities of *Silybum marianum* mediated biosynthesized copper oxide nanoparticles, RSC Adv. 12 (2022) 14069–14083.
[101] J. Wongpreecha, D. Polpanich, T. Suteewong, C. Kaewsaneha, P. Tangboriboonrat, One-pot, large-scale green synthesis of silver nanoparticles-chitosan with enhanced antibacterial activity and low cytotoxicity, Carbohydr. Polymers 199 (2018) 641–648.
[102] A. Nair, C. Jayakumari, P. Jabbar, R. Jayakumar, N. Raizada, A. Gopi, G. S. George and T. Seena, Prevalence and associations of hypothyroidism in Indian patients with type 2 diabetes mellitus, J. Thyroid Res. 2018 (2018) 7.
[103] S. Ghosh, P. More, R. Nitnavare, S. Jagtap, R. Chippalkatti,A. Derle, R. Kitture, A. Asok, S. Kale and S. Singh, Antidiabetic and antioxidant properties of copper nanoparticles synthesized by medicinal plant *Dioscorea bulbifera*, J. Nanomed. Nanotechnol. S6 (2015) 1–9.
[104] U. Shwetha, M. Latha, C. R. Kumar, M. Kiran, H. Onkarappa and V. S. Betageri, Potential antidiabetic and anticancer activity of copper oxide

nanoparticles synthesised using *Areca catechu* leaf extract, Adv. Nat. Sci.: Nanosci. Nanotechnol. 12 (2021) 025008.

[105] W.D. Seo, J.H. Kim, J.E. Kang, H.W. Ryu, M.J. Curtis-Long, H.S. Lee, M.S. Yang, K.H. Park, Sulfonamide Chalcone as a new class of alpha-glucosidase inhibitors, Bioorg. Med. Chem. Lett. 15 (24) (2005) 5514–5516.

[106] J.P. Saludes, S.C. Lievens, T.F. Molinski, Occurrence of the alpha-glucosidase inhibitor 1,4-Dideoxy-1,4-imino-D-arabinitoland related iminopentitols in marine sponges, J. Natural Products. 70 (3) (2007) 436–438.

[107] N.U. Islam, R. Amin, M. Shahid, M. Amin, S. Zaib and J. Iqbal, A multi-target therapeutic potential of *Prunus domestica* gum stabilized nanoparticles exhibited prospective anticancer, antibacterial, urease-inhibition, anti-inflammatory and analgesic properties, BMC Complementary Altern. Med. 17 (2017) 1–17.

[108] Sachan S. and A. Singh, Lipase enzyme and its diverse role in food processing industry, Everyman's Sci. 4 (2015) 214–218.

[109] M. I. Choudhary, M. Ali, A.-T. Wahab, A. Khan, S. Rasheed,S. L. Shyaula and A.-U. Rahman, New antiglycation and enzyme inhibitors from *Parmotrema cooperi*, Sci. China: Chem. 54 (2011) 1926–1931.

[110] W.I. Abdel-Fattah, G.W. Ali, Anti-cancer activities of silver nanoparticles, J. Appl. Biotechnol. Bioeng. 5 (2018) 00116.

[111] P. Rameshthangam, J.P. Chitra, Synergistic anticancer effect of green synthesized nickel nanoparticles and quercetin extracted from *Ocimum sanctum* leaf extract, J. Materials Sci & Tech. 34 (2018) 508–522.

[112] F. Ibraheem, M.H. Aziz, M. Fatima, F. Shaheen, S.M. Ali, Q. Huang, In vitro Cytotoxicity, MMP and ROS activity of green synthesized nickel oxide nanoparticles using extract of *Terminalia chebula* against MCF-7 cells, Materials Lett. 234 (2019) 129–133.

[113] R. Sankar, R. Maheswari, S. Karthik, *et al*., Anticancer activity of *Ficus religiosa* engineered copper oxide nanoparticles, Mat Sci Eng C. 44 (2014) 234–239.

[114] M. Baghayeri, B. Mahdavi, Z. Hosseinpor-Mohsen Abadi, S. Farhadi, Green synthesis of silver nanoparticles using water extract of *Salvia leriifolia*: Antibacterial studies and applications as catalysts in the electrochemical detection of nitrite, Appl. Organomet. Chem. 32 (2018) e4057.

[115] K. Sridhar, A.L. Charles, In vitro antioxidant activity of Kyoho grape extracts in DPPH and ABTS assays: Estimation methods for EC50 using advanced statistical programs, Food Chem. 275 (2019) 41–49. doi: 10.1016/j.foodchem.2018.09.040.

[116] R. Subramanian, P. Subbramaniyan, V. Raj, Antioxidant activity of the stembark of *Shorea roxburghii* and its silver reducing power, Springer Plus 2 (1) (2013) 28.

[117] P. Khandel, S.K. Shahi, D.K. Soni, R.K. Yadaw and L. Kanwar, *Alpinia calcarata*: potential source for the fabrication of bioactive silver nanoparticles, Nano Convergence 5 (2018) 37. https://doi.org/10.1186/s40580-018-0167-9.

[118] M. Shah, S. Nawaz, H. Jan, N. Uddin, A. Ali, S. Anjum,N. Giglioli-Guivarc'h, C. Hano and B. H. Abbasi, Synthesis of bio-mediated silver nanoparticles from *Silybum marianum* and their biological and clinical activities, Mater. Sci. Eng., C. 112 (2020) 110889.

[119] S. Sangami, B. Manu, Synthesis of green iron nanoparticles using laterite and their application as a Fenton-like catalyst for the degradation of herbicide ametryn in water, Environ Technol Innov. 8 (2017) 150–163.

[120] L. Katata-Seru, T. Moremedi, O.S. Aremu, I. Bahadur, Green synthesis of iron nanoparticles using *Moringa oleifera* extracts and their applications: Removal of nitrate from water and antibacterial activity against *Escherichia coli*, J Mol Liq. 256 (2018) 296–304.

[121] N. Beheshtkhoo , M.A.J. Kouhbanani, A. Savardashtaki, A.M. Amani, S. Taghizadeh, Green synthesis of iron oxide nanoparticles by aqueous leaf extract of *Daphne mezereum* as a novel dye removing material, Appl. Phys A. 124 (2018) 363–369.

[122] I.A. Radini, N. Hasan, M.A. Malik, Z. Khan, Biosynthesis of iron nanoparticles using *Trigonella foenum-graecum* seed extract for photocatalytic methyl orange dye degradation and antibacterial applications, J Photochem Photobiol B. 183 (2018) 154–163.

[123] C.A. Sousa, H.M. Soares and E.V. Soares, Nickel oxide (NiO) nanoparticles induce loss of cell viability in yeast mediated by oxidative stress, Chem. Res. Toxicol. 31 (2018) 658–665.

[124] W. Jansen, J. Van Der Bruggen, J. Verhoef, A. Fluit, Bacterial resistance: a sensitive issue: complexity of the challenge and containment strategy in Europe, Drug Resist. Updat. 9 (2006) 123–133.

[125] M. Behravan, A.H. Panahi, A. Naghizadeh, M. Ziaee, R. Mahdavi, A. Mirzapour, Facile green synthesis of silver nanoparticles using *Berberis vulgaris* leaf and root aqueous extract and its antibacterial activity, Internat J. Biological Macromol. 124 (2019) 148–154.

[126] B.S. Atiyeh, M. Costagliola, S.N. Hayek, S.A. Dibo, Effect of silver on burn wound infection control and healing: review of the literature, Burns 33 (2007) 139–148.
[127] M.M. Mohamed, S.A. Fouad, H.A. Elshoky, G.M. Mohammed, T.A. Salaheldin, Antibacterial effect of gold nanoparticles against *Corynebacterium pseudotuberculosis*, Int. J. Vet. Sci. Med. 5 (1) (2017) 23–29.
[128] P. Senthilkumar, L. Surendran, B. Sudhagar, D. S. Ranjith Santhosh Kumar, Facile green synthesis of gold nanoparticles from marine algae *Gelidiella acerosa* and evaluation of its biological potential, SN Applied Sci. 1 (2019) 284. https://doi.org/10.1007/s42452-019-0284-z.
[129] I. Sondi and B. Salopek-Sondi, Silver nanoparticles as antimicrobial agent: a case study on *E. coli* as a model for Gram-negative bacteria, J. Colloid Interface Sci. 275 (2004) 177–182.
[130] G. Ren, D. Hu, E. W. Cheng, M.A. Vargas-Reus, P. Reip and R.P. Allaker, Characterisation of copper oxide nanoparticles for antimicrobial applications, Int. J. Antimicrob. Agents. 33 (2009) 587–590.
[131] S. Jadhav, S. Gaikwad, M. Nimse and A. Rajbhoj, Copper oxide nanoparticles: synthesis, characterization and their antibacterial activity, J. Cluster Sci. 22 (2011) 121–129.
[132] Y.-N. Chang, M. Zhang, L. Xia, J. Zhang and G. Xing, The toxic effects and mechanisms of CuO and ZnO nanoparticles, Materials 5 (2012) 2850–2871.
[133] L. Karygianni, Z. Ren, H. Koo, T. Thurnheer, Biofilm Matrixome: Extracellular components in structured microbial communities, Trends Microbiol. 28 (8) (2020) 668–681.
[134] A.S. Joshi, P. Singh, I. Mijakovic, Interactions of gold and silver nanoparticles with bacterial biofilms: Molecular interactions behind inhibition and resistance, Int. J. Mol. Sci. 21 (20) (2020) 7658.
[135] S. Oliver, H. Wagh, Y. Liang, S. Yang and C. Boyer, Enhancing the antimicrobial and antibiofilm effectiveness of silver nanoparticles prepared by green synthesis, J. Mater. Chem. B.6 (2018) 4124-4138.
[136] M.A. El-ghamry, K.M. Nassir, F.M. Elzawawi, A.A. Abdel Aziz, S.M. Abu-El-Wafa, Novel nanoparticle-size metal complexes derived from acyclovir. Spectroscopic characterization, thermal analysis, antitumor screening, and DNA cleavage, as well as 3D modeling, docking, and electrical conductivity studies, J. Molecular Struct. 1235 (2021) 130235.
[137] F. Gulbagca, A. Aygün, M. Gülcan, S. Ozdemir, S. Gonca, F. Şen, Green synthesis of palladium nanoparticles: Preparation, characterization, and

investigation of antioxidant, antimicrobial, anticancer, and DNA cleavage activities, Appl Organomet Chem. (2021) e6272.https://doi.org/10.1002/aoc.6272.

[138] M.Y. Begum, Y. Alhamhoom and A. Roy, Study of antimicrobial and DNA cleavage property of biocompatible silver nanoparticles prepared by using *Ficus carica* L., Materials Res Innovat. (2020) DOI: 10.1080/14328917.2020.1753335.

[139] S. Ravichandran, V. Paluri, G. Kumar, K. Loganathan, B.R. Kokati Venkata, A novel approach for the biosynthesis of silver oxide nanoparticles using aqueous leaf extract of *Callistemon lanceolatus* (Myrtaceae) and their therapeutic potential, J. Exp. Nanosci. 11 (2016) 445–458.

[140] E. Dilshad, M. Bibi, N.A. Sheikh, K.F. Tamrin, Q. Mansoor, Q. Maqbool and M. Nawaz, Synthesis of functional silver nanoparticles and microparticles with modifiers and evaluation of their antimicrobial, anticancer, and antioxidant activity, J. Funct. Biomater. 11 (2020) 76; doi:10.3390/jfb11040076.

[141] Z. He, S. Mahmud, Y. Yang, L. Zhu, Y. Zhao, Q. Zeng, Z. Xiong, S. Zhao, Polyvinylidene fluoride membrane functionalized with zero valent iron for highly efficient degradation of organic contaminants, Separ. Purif. Technol. 250 (2020a) 117266.

[142] Z. He, S. Mahmud, S. Zhao, Y. Yang, L. Zhu, Y. Zhao, Q. Zeng, Z. Xiong, C. Hu, Hierarchically active poly(vinylidene fluoride) membrane fabricated by in situ generated zero-valent iron for fouling reduction, ACS Appl. Mater. Interf. 12 (9) (2020b) 10993–11004.

[143] Y. Zhong, S. Mahmud, Z. He, Y. Yang, Z. Zhang, F. Guo, Z. Chen, Z. Xiong, Y. Zhao, Graphene oxide modified membrane for highly efficient wastewater treatment by dynamic combination of nanofiltration and catalysis, J. Hard Mater. 397 (2020) 122774.

[144] H. Wang, G. Zhang, R. Mia, W. Wang, L. Xie, S. Lü, S. Mahmud, H. Liu, Bioreduction (Ag^{+} to Ag^{0}) and stabilization of silver nanocatalyst using hyaluronate biopolymer for azo-contaminated wastewater treatment, J. Alloys Comp. 894 (2022) 162502.

[145] S. Pandey, J.Y. Do, J. Kim, M. Kang, Fast and highly efficient catalytic degradation of dyes using κ-carrageenan stabilized silver nanoparticles nanocatalyst, Carbohydr. Polym. 230 (2020) 115597.

[146] J. Li, C.-Y Liu, Y. Liu, Au/graphene hydrogel: synthesis, characterization and its use for catalytic reduction of 4-nitrophenol, J. Mater. Chem. 22 (2012) 8426–8430.